Front. Phys., 2014, 9(3): 303–322
DOI 10.1007/s11467-013-0343-7

REVIEW ARTICLE

Hierarchical nanowires for high-performance electrochemical energy storage

Shuo Li (李硕), **Yi-Fan Dong** (董轶凡), **Dan-Dan Wang** (王丹丹), **Wei Chen** (陈伟)*, **Lei Huang** (黄磊), **Chang-Wei Shi** (石长玮), **Li-Qiang Mai** (麦立强)†

State Key Laboratory of Advanced Technology for Materials Synthesis and Processing, WUT–Harvard Joint Nano Key Laboratory, Wuhan University of Technology, Wuhan 430070, China

*Corresponding authors. E-mail: †mlq518@whut.edu.cn, *chenwei_juan@sina.com*

Received March 31, 2013; accepted May 8, 2013

Nanowires are promising candidates for energy storage devices such as lithium-ion batteries, supercapacitors and lithium-air batteries. However, simple-structured nanowires have some limitations hence the strategies to make improvements need to be explored and investigated. Hierarchical nanowires with enhanced performance have been considered as an ideal candidate for energy storage due to the novel structures and/or synergistic properties. This review describes some of the recent progresses in the hierarchical nanowire merits, classification, synthesis and performance in energy storage applications. Herein we discuss the hierarchical nanowires based on their structural design from three major categories, including exterior design, interior design and aligned nanowire assembly. This review also briefly outlines the prospects of hierarchical nanowires in morphology control, property enhancement and application versatility.

Keywords hierarchical nanowires, exterior design, interior design, electrochemical performance, energy storage

PACS numbers 61.46.-w, 61.46.Km, 73.63.-b, 82.45.Yz

Contents

1 Introduction

Energy storage is one of the great challenges in the 21st century. In response to the needs of emerging social and ecological concerns, it is now essential to explore new, low-cost and environmentally friendly energy storage systems in this field. Lithium-ion batteries (LIBs), supercapacitors and lithium air batteries are at the frontier of this research effort, as they play important roles in our daily lives by powering numerous portable consumer electronic devices (such as cell phones, PDAs, laptops) and even current electric vehicles [1–7].

A typical commercial lithium-ion battery is comprised of a negative electrode (anode), a positive electrode (cathode), and a non-aqueous liquid electrolyte between them. On charging, lithium ions are extracted from the cathode intercalation host, pass through the electrolyte, and intercalate into the anode. Discharge is the reverse of this process [8].

Supercapacitors are capacitors that contain an electrolyte solution in place of a dielectric layer. These devices can be composed of the same material for the cathode and anode as in a symmetric device or different materials as in an asymmetric device. Supercapacitors can be divided into two separate types depending on their charge storage mechanism: Electrochemical Double Layer Capacitors (EDLCs) and pseu-

Frontiers of Physics

docapacitors. EDLCs store their charge in the double layer that forms between the electrode material and the electrolyte upon charging. Pseudocapacitors do not rely on the traditional charge separation mechanism that is typical of a capacitor. They rely on a fast surface or near-surface faradic charge-transfer mechanism which gives them their "pseudo"-capacitive behavior. Transition metal oxides such as RuO_2, Fe_3O_4, and MnO_2 along with conductive polymers are the typical materials used for these devices.

Recently, lithium-air batteries have captured worldwide attention due to their ultrahigh energy density among the chemical batteries. The Li-air cell uses Li as the anode, and a cathode consists of a porous conductive composite, usually carbon and a catalyst, which is flooded with electrolyte. Oxygen from the atmosphere dissolves in the electrolyte and is reduced. On discharge, Li ions pass through the electrolyte and react with the reduced oxygen. At the positive electrode, O_2 from the atmosphere enters the porous cathode, dissolves in the electrolyte within the pores and is reduced at the electrode surface on discharge. The process is reversed on charging. Either aqueous or nonaqueous electrolytes can be used. For the former, a Li-ion conducting solid electrolyte separates the metallic Li from the aqueous electrolyte [9, 10].

The future will require the electrochemical energy storage devices to be able to achieve extraordinarily high energy densities at high rate capabilities. The performance of lithium ion batteries, supercapacitors and Li-air batteries depends intimately on the properties of their electrodes or catalyst materials.

Because of the specific characteristics intrinsically associated with nanostructured materials, such as small size effect, surface effect, quantum size effect and quantum tunnel effect, nanoscale materials have been valuable candidates for electrochemical energy storage [11–17]. As for 1D nanostructured materials, they not only exhibit outstanding electronic and energy storage properties but also serve as the critical components in the potential nanoscale device applications. Until now, 1D nanostructured materials, ranging from nanowires, nanotubes, nanorods to nanobelts (in this review, all of these are noted as nanowires) have extended a new direction for improving both capacity and lifetime of these energy storage devices. Compared with bulk materials, nanowires have shorter Li-ion insertion/extraction distance and shorter path length for electronic transport, which permit the operation with low lithium ion conductivity and electronic conductivity, respectively. Moreover, the merits of facile strain relaxation upon charging/discharging for long cycling life, very large surface to volume ratio to contact the conductive additives endow nanowires ideal candidates for electrodes in electrochemical energy storage [18–23].

It is a trend that nanowire building blocks with novel structures and multiple functionalities are developed with both enhanced performance and applications. A typical representative for this is hierarchical nanowire assembly. However, there have been rare reviews for hierarchical nanowire classification, assembly, performance and prospects in electrochemical energy storage applications. In this review, we concentrate on the advantages for hierarchical nanowires and the recent progresses of using hierarchical nanowire electrode materials for applications in electrochemical energy storage devices. Assembling building blocks on synthesized nanowires are defined as exterior design and this method is widely used as it combines the synergistic effect of both materials. Contrarily, a method which the inner properties such as component distribution, morphology, concentration of a nanowire are designed or modified is defined as interior design. Besides, nanowires can be assembled in alignment to form aligned nanowire arrays to enhance the performance.

Thus, in the following discussion, we will state the advantages of hierarchical nanowires over simple-structured nanowires by *in situ* characterizing the nanowire transformation during electrochemical tests, and then classify the hierarchical nanomaterials into three major categories based on their structural design, i.e. exterior design, interior design and aligned nanowire assembly (Fig. 1). In exterior design and interior design categories, the structural complexity is gradually increased, from coax ial nanowires to branched nanowires in exterior design and from substructured nanowires to gradient nanowires in interior design. At last, the prospect of hierarchical nanowires in energy storage systems will be elaborated.

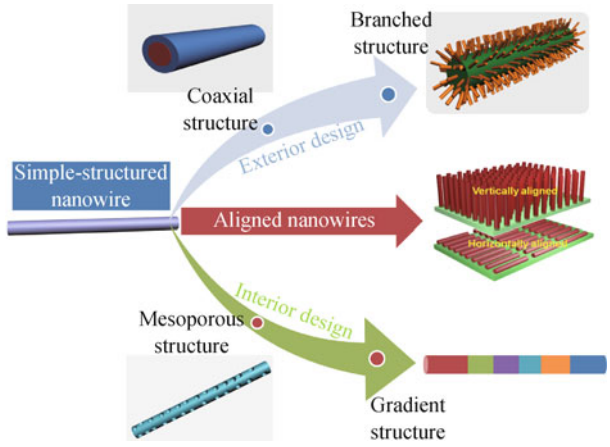

Fig. 1 Schematic illustration of assembling strategies of hierarchical nanowires.

2 Advantages of assembling hierarchical nanowires

As mentioned above, nanowires, especially simple-structured nanowires, may not be able to fulfill the requirements of future electrochemical energy storage devices because of some of their intrinsic limitations such as conductivity decrease during cycling, poor cyclability due to lithiation/delithiation-induced structure degradation, low conductivities as well as slow kinetics (low energy densities at high charge/discharge rates) and weak mechanical stabilities which cannot be simply altered and enhanced by just transforming them into nanomaterials. Moreover, nanowires may have significant side reactions with the electrolyte and self-aggregation due to their high surface area and high surface energy, which will lead to irreversibility and thus poor cycle life. These limitations have been widely reported by both theories and experiments [24–31]. Besides, the *in situ* characterization of nanowires simulating the electrochemical reactions needs to be performed to explore the intrinsic limitations and hence the solutions of enhancements.

Researchers have explored various methods to study the intrinsic reasons for capacity fading and tried to figure out the solutions. Mai *et al.* [32] have firstly reported the fabrication of single nanowire all-solid electrical energy storage devices to *in situ* characterize the conductance change of a single nanowire during lithiation/delithiation. The device contains just one nanowire as either cathode or anode and uses classical materials for counter electrodes and electrolytes [Fig. 2(a)]. No binders or conductive carbon additives were introduced into the systems. Single nanostructure transport study can be combined with electrode electrochemical performance test so that the relationship between electrode material composition, structure, transport properties, charge/discharge status and electrochemical performance can be studied at single nanowire level to reveal the intrinsic reason for fast capacity fading. During battery operation, conductivity of the single vanadium oxide nanowire was also investigated. The transport properties of the same single nanowire at different charge/discharge status are shown [Fig. 2(b)–(f)]. Initially, the vanadium oxide nanowire was highly conductive [Fig. 2(b)], agreeing with its original intact crystal structures. Along with lithium ion intercalation by shallow discharge with 100 pA for 200 seconds, the nanowire conductance was decreased over two orders [Fig. 2(c)]. The conductance change can be restored to previous scale upon lithium ions deintercalation with shallow charge with –100 pA for 200 seconds [Fig. 2(d)] indicating reversible structure change. However, when the battery device was deeply discharged with 100 pA for 400 seconds, the nanowire conductance dropped for over five orders [Fig. 2(e)]. This change was permanent and could not be recovered even after deep charging with –100 pA for 400 seconds, indicating that permanent structure change happens when too many lithium ions were intercalated into the vanadium oxide layered structures [Fig. 2(f)]. Based on the single nanowire electrode platform, the material electrical properties, crystal structure change and electrochemical charge/discharge status are clearly correlated.

Three months later after Mai *et al.*'s work, Huang *et al.* [33] from Sandia National Laboratories have developed a nanoscale electrochemical device consisting of a single tin dioxide (SnO_2) nanowire anode, an ionic liquid electrolyte, and a bulk lithium cobalt dioxide ($LiCoO_2$) cathode inside a transmission electron microscope, and the *in situ* observation of lithiation of the SnO_2 nanowire during electrochemical charging was achieved [Fig. 2(g)]. Upon charging, a reaction front propagated progressively along the nanowire, causing the nanowire to swell, elongate, and spiral. The observations demonstrate that the lithiation-induced volume expansion, plasticity, and pulverization of electrode materials are the major mechanical effects that plague the performance and lifetime of high-capacity anodes in Li-ion batteries [Fig. 2(h)–(s)]. These results correspond well to Mai's work and indicate that the simple-structured nanowires suffer great degradation during lithium intercalation/deintercalation.

In order to overcome the above limitations of using simple-structured electrode materials, hierarchical nanowires have been a focus of the nanomaterial energy storage research field as they share many merits and advantages such as high surface/body ratios, large surface areas, better permeabilities and more surface active sites, and have a great potential in energy storage and electrochemical applications [34–37].

3 Exteriorly designed hierarchical nanowires

There have existed numerous methods to synthesize nanowire materials, such as the hydrothermal methods, micro emulsion method, electrospinning and template method. Assemblies of other components like coating layers or branch nanowires can be achieved based on the as-synthesized nanowires as backbones, and have been widely reported. In this part, we define this kind of assembled hierarchical nanowires as exterior design including coaxial nanowires and branched nanowires, and provide an overview of recent progresses of exterior design of hierarchical nanowires in electrochemical energy storage

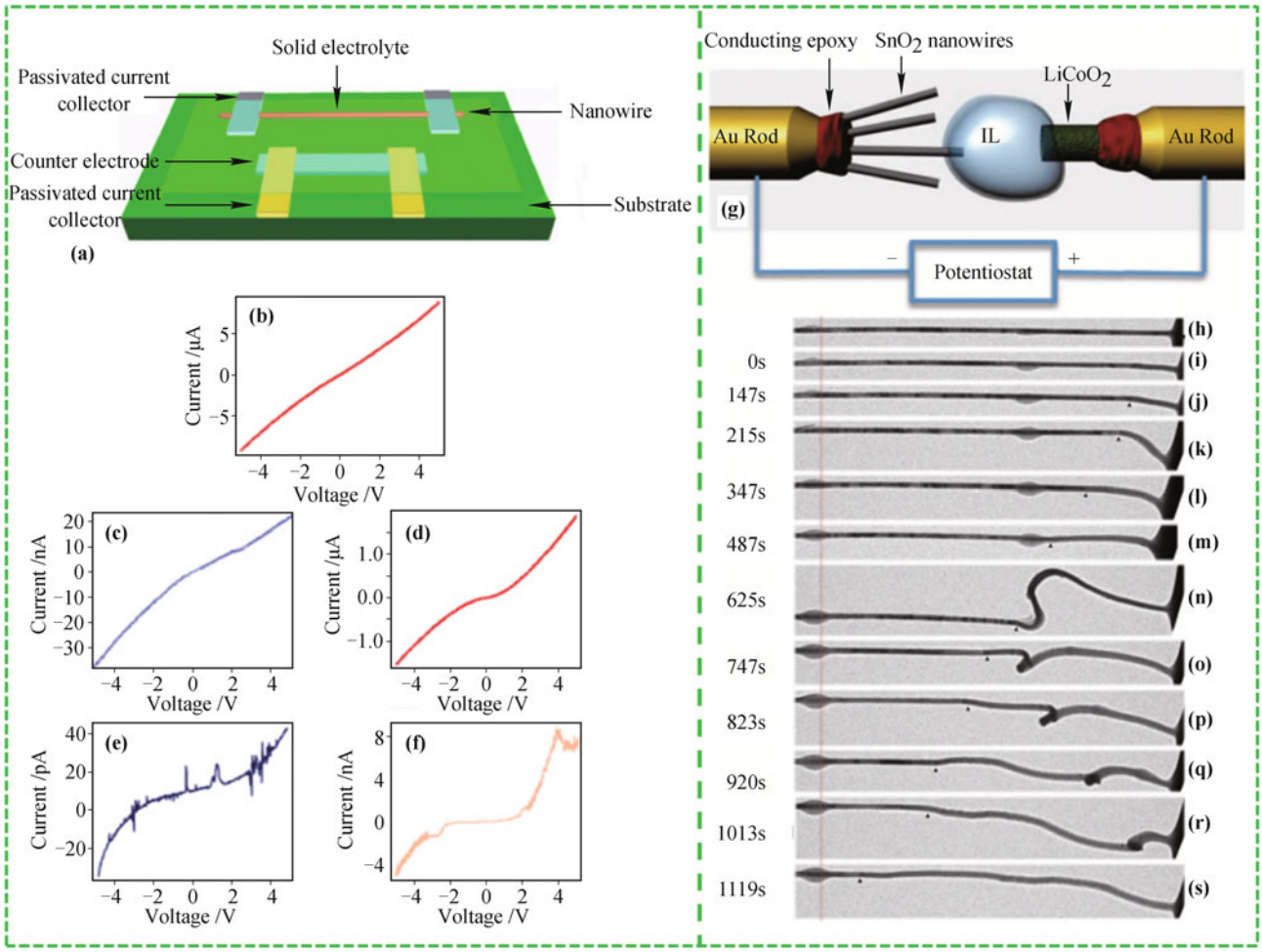

Fig. 2 **(a)** Schematic diagram of a single nanowire electrode device design. **(b)** Single vanadium oxide nanowire transport properties at initial state; **(c)** after Li^+ ion intercalation (shallow discharge with 100 pA for 200 seconds); **(d)** after Li^+ ion deintercalation (shallow charge with –100 pA for 200 seconds); **(e)** after deep discharge with 100 pA for 400 seconds; **(f)** after deep charge with –100 pA for 400 seconds. **(g)** Schematic of SnO_2 nanowire electrode. **(h)**–**(s)** Time-lapse structure evolution of a SnO_2 nanowire anode during charging at –3.5 V against a $LiCoO_2$ cathode. **(a)**–**(f)** Reproduced from Ref. [32], Copyright © 2010 American Chemical Society; **(g)**–**(s)** Reproduced from Ref. [33], Copyright © 2010 Nature Publishing Group.

device applications.

3.1 Coaxial nanowires

Coaxial nanowires, or core-shell nanowires, are relatively simple structures among all the hierarchical nanowires. Coating another material on the backbone nanowires is usually the most facile and common way to synthesize coaxial nanowires. It is an effective method to utilize both materials synergistically and enhance the performance, and this method has been widely used in variety of research fields such as photovoltaics [38–46], biotechnology [47], nanoelectronics [48–56] and catalysts [57], etc. Especially in electrochemical energy storage applications, coaxial structured nanowires are often chosen as the method to enhance the electrical conductivity, prevent aggregation, improve chemical stability, and buffer the stress of the inner nanoscale active material [58, 59] [Fig. 3(a)]. The coating layer should be permeable to lithium ions, thus the lithium ion diffusion in the active materials can be maintained. Moreover, the coating layer is always of uniformity, flexibility and high-conductivity, thus the backbone nanowires can be effectively protected from side reactions with electrolyte and structure degradation, and the better electrochemical performance can be achieved.

Carbon and conductive polymers are usually chosen as the coating layers, as well as some metals or metal oxides. Zhang *et al.* [60] have reported carbon-coated Fe_3O_4 nanospindles by partial reduction of monodispersed hematite nanospindles with carbon coatings. The carbon coated Fe_3O_4 spindles have the length of about 500 nm and an aspect ratio of about 4. The outer carbon layers with uniform and continuous features improve the

electrochemical performance in several ways, including maintaining the integrity of particles, increasing the electronic conductivity of electrodes leading to the formation of uniform and thin solid-electrolyte interface (SEI) films on the surface, and stabilizing the as-formed SEI films [Fig. 3(b)]. Reddy *et al.* [61] have combined simple vacuum infiltration and chemical vapor deposition techniques to prepare MnO_2/CNT hybrid coaxial nanotube arrays using porous alumina templates. The coaxial hybrid structure formed by the highly conductive CNT core offers enhanced electronic transport to the MnO_2 shell and acts as a buffer to alleviate the volume expansion [Fig. 3(c)]. Luo *et al.* [62] have successfully synthesized large-scale tin-core/carbon-sheath coaxial nanocables with uniform diameter and high aspect ratio in a controlled fashion by a simple chemical vapor deposition (CVD) process using reduced graphene (RGO) based hybrid material as an efficient platform. The carbon sheath was approximately 5 nm thick and made up of staggered, shortened graphene-like sheets, and the tin and carbon element mapping for a single nanocable clearly shows the tin-core/carbon-sheath coaxial structure [Fig. 3(d)]. Yuan *et al.* [63] have proposed a special route, using R-FeOOH nanorods coated with carbon layers as precursors, to prepare Fe_3O_4@C microcapsules, in which mesopores are generated during the sintering procedure after the carbon coating. This unique structure endows the Fe_3O_4@C microcapsules excellent electrochemical performance of a specific capacity of 1010 mAh/g after 50 cycles at a current density of 92.8 mA/g [Fig. 3(e)]. Some oxides are also commonly used as coating layers. Wu *et al.* [64] have fabricated a double-walled Si-SiO_x nanotube (DWSiNT) anode structure in which the inner wall is active silicon and the outer wall is confining SiO_x, which allows lithium ions to pass through. Due to the existence of the SiO_x shell, the electrolyte only contacts the outer surface and is not able to enter the inner hollow space, thus the SEI layer growth only occurs at the outer wall of the Si nanotube. The DWSiNT structure provides two attractive features as an anode material: the static outer surface allows for the development of a stable SEI and the inner space allows for free volume expansion of the silicon without mechanical breaking [Fig. 3(f)]. Kim *et al.* [65] have reported a novel SnO_2-In_2O_3 coaxial nanowires structure by thermal evaporation method. The surface modification of the SnO_2 nanowires by In_2O_3 leads to higher electronic conductivity because of the formation of Sn-doped In_2O_3 (ITO) caused by the incorporation of Sn into the In_2O_3 lattice during the nucleation and growth of the In_2O_3 shell nanostructures, and the conductivity of the In_2O_3/SnO_2 nanowire is 2 orders of magnitude better than that of the pure SnO_2 nanowire which provides the SnO_2-In_2O_3 nanowires with an outstanding lithium storage capacity [Fig. 3(g)].

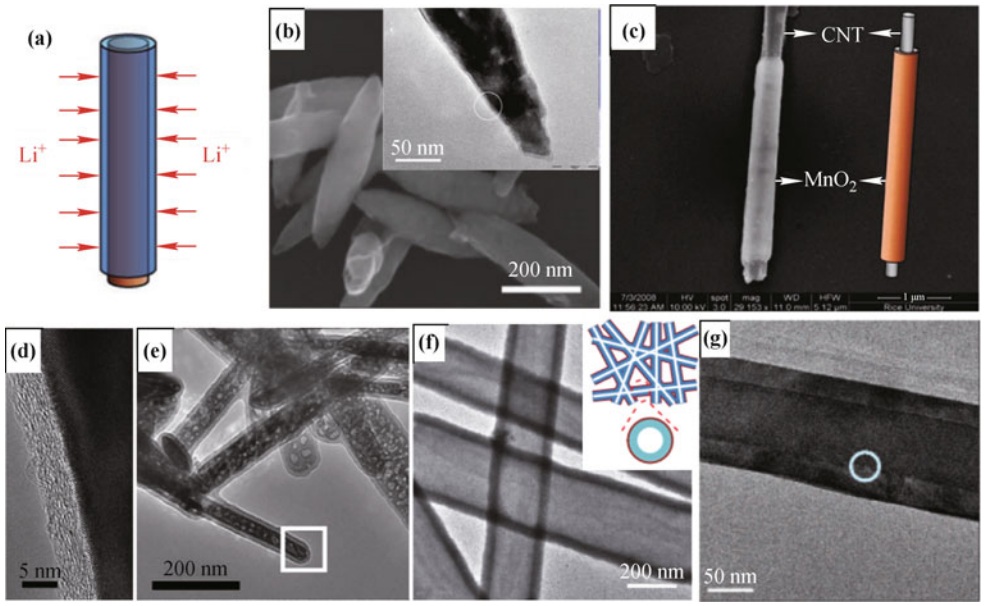

Fig. 3 **(a)** Schematic of coating layers functions during lithium ion diffusion in coaxial nanowires; **(b)** Scanning electron microscopic (SEM) and Transmission electron microscopic (TEM) images of carbon coated Fe_3O_4 nanospindles. Reproduced from Ref. [60], Copyright © 2009 American Chemical Society. **(c)** SEM image of coaxial MnO_2/Carbon nanotube array. Reproduced from Ref. [61], Copyright © 2012 Wiley-VCH. **(d)** TEM image of uniform tin-core/carbon-sheath coaxial nanocables. Reproduced from Ref. [62], Copyright © 2012 Nature Publishing Group. **(e)** TEM image of mesoporous Fe_3O_4@C nanorods. Reproduced from Ref. [63], Copyright © 2011 American Chemical Society. **(f)** TEM image of double-walled silicon nanotube. Reproduced from Ref. [64], Copyright © 2007 American Chemical Society. **(g)** SEM image of coaxial SnO_2-In_2O_3 heterostructured nanowires. Reproduced from Ref. [65], Copyright © 2012 American Chemical Society.

The coaxial nanowires can even be extended to triaxial nanowires. Mai *et al.* [66] have synthesized the silver vanadium oxides/polyaniline (SVO/PANI) triaxial nanowires by combining *in situ* chemical oxidative polymerization and interfacial redox reaction based on β-$AgVO_3$ nanowires [Fig. 4(a)]. The presence of the Ag particle in a transmission electron microscopy image confirms the occurrence of the redox reaction [Fig. 4(b)]. The triaxial nanowires exhibit enhanced electrochemical performance. Cyclic voltammetry (CV) measurement shows that the triaxial nanowires exhibit much higher current density than that of β-$AgVO_3$ nanowires, which indicates faster kinetics and higher capacity. The cycling stability is also improved after conductive polymer coating, and the enhanced electrochemical performance of the triaxial nanowires may result from the decrease of the charge transfer resistance from 1388 to 839.7 Ω [Fig. 4(c)]. The higher capacity and better cycling stability of SVO/PANI nanowires were demonstrated as cathode materials of a rechargeable Li-ion Battery. A 50 wt % SVO/PANI triaxial nanowire cathode possesses the highest initial and 20th discharge capacities, which are 211 and 131 mAh/g with 20th cycle capacity retention of 62%, both higher than those of β-$AgVO_3$ nanowires, which are 199 and 76 mAh/g with 20th cycle capacity retention of 41.7%. This *in situ* chemical oxidative polymerization coating method can be applied to other polymer coatings and has been realized in polythiophene (PTh) coated MoO_3 nanowires [67] with enhanced electrochemical cyclability.

The coating layers can be further decorated or improved. Based on the previous reports, Mai *et al.* [68] have also designed the heterostructured nanomaterial with poly (3, 4-ethylenedioxythiophene) (PEDOT) as the shell and MnO_2 nanoparticles as the protuberance in the shell and synthesized the novel cucumber-like MnO_2 nanoparticles enriched vanadium pentoxide/PEDOT coaxial nanowires by combining the *in situ* chemical oxidative polymerization with facile soaking process [Fig. 5(a), (b)]. The heterostructured nanomaterial exhibits enhanced electrochemical cycling performance with the decreases of capacity fading during 200

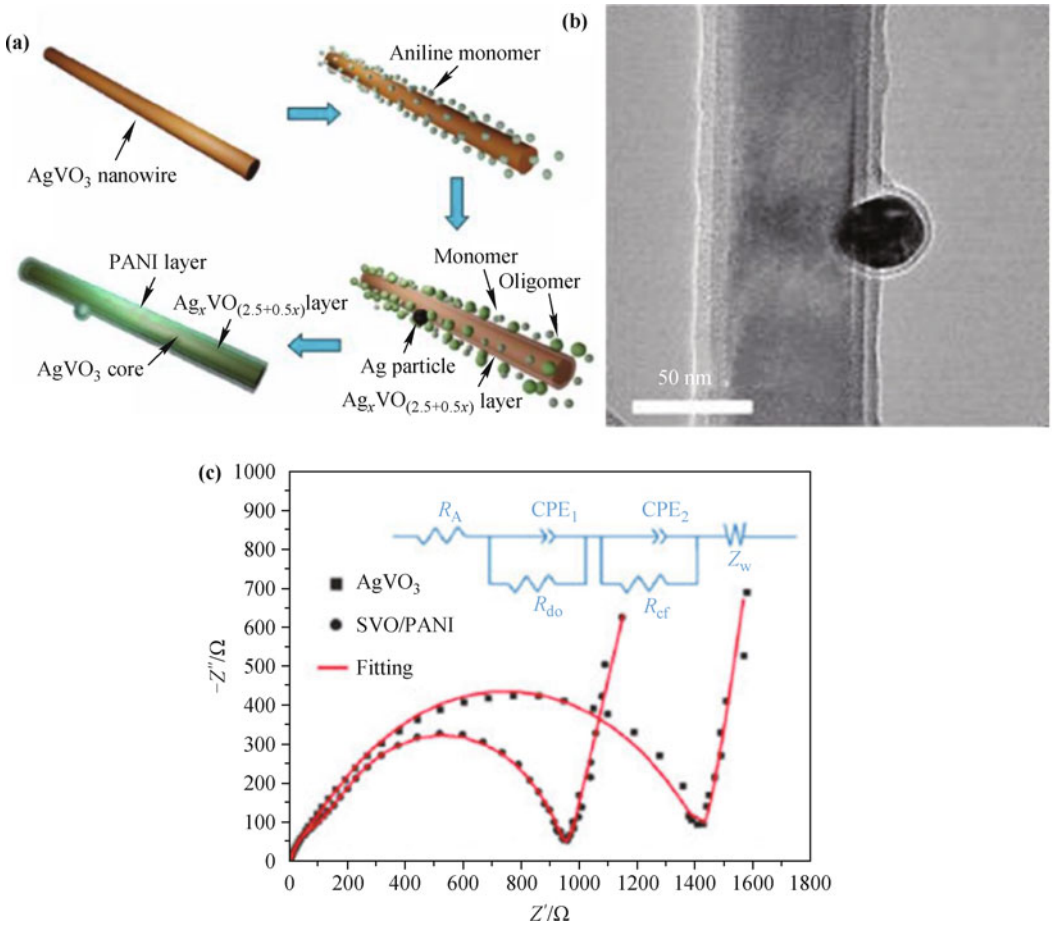

Fig. 4 **(a)** Schematic illustration of the formation of SVO/PANI triaxial nanowire. **(b)** TEM images of SVO/PANI triaxial nanowires. **(c)** AC impedance spectra curve of β-$AgVO_3$ nanowires and SVO/PANI triaxial nanowires. Reproduced from Ref. [66], Copyright © 2011 American Chemical Society.

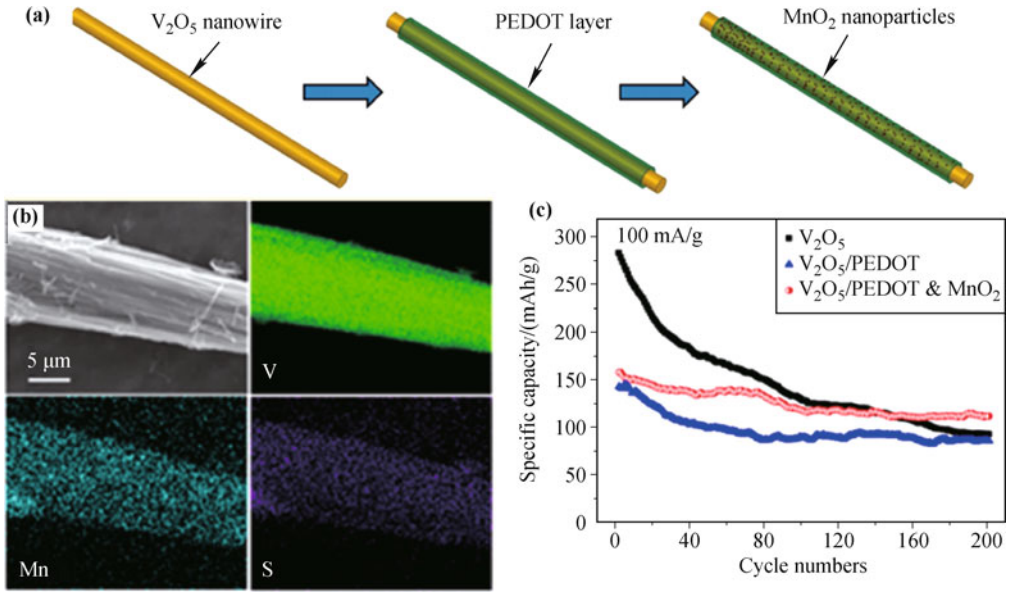

Fig. 5 **(a)** Schematic illustration of the synthesis of V_2O_5/PEDOT & MnO_2 NWs. **(b)** Energy Dispersive Spectrometer (EDS) mapping of V, Mn, and S from V_2O_5/PEDOT&MnO_2 NWs. **(c)** Cycling performance of V_2O_5, V_2O_5/PEDOT and V_2O_5/PEDOT&MnO_2 at 100 mA/g. Reproduced from Ref. [68], Copyright © 2013 American Chemical Society.

cycles from 0.557% to 0.173% over V_2O_5 nanowires at the current density of 100 mA/g, which is proven to be an effective technique for improving the electrochemical cycling performance and stability of nanowire electrodes especially at low rate for application in rechargeable lithium batteries due to the quantum dots of MnO_2 and biomimetic structure [Fig. 5(c)].

The coaxial structure has also been applied to supercapacitors. Liu *et al.* [69] have fabricated MnO_2/PEDOT coaxial nanowires by a one-step coelectrodeposition method, the MnO_2 core is utilized for its high energy density, while the PEDOT shell is applied for its high conductivity and its porous and flexible nature [Fig. 6(a), (b)]. The PEDOT shell facilitates electron transport and ion diffusion into the energy dense MnO_2 core and protects the core from structural collapse and breaking. These combined properties result in a synergic composite that has very high specific capacitances at high current densities as opposed to pure MnO_2 nanowires and PEDOT nanowires, and a MnO_2 thin film [Fig. 6(c)].

In general, compared with simple-structured nanowires, the coaxial nanowires exhibit better electrochemical performance in energy storage devices and this method is widely used and applied in many fields because of its facility and synthetic variety.

3.2 Branched nanowires

Fabricating coaxial nanowires is a facile and efficient way to realize enhanced performance, yet it still has some limitations such as the coating layer may restrain the reactivity of the core materials and may increase the mass of inert materials. Thus, branched or tree-like nanowire structures have been demonstrated to get rid of the limitations listed above [36, 70–73]. Branched nanowires not only work well against the aggregation issue, but also

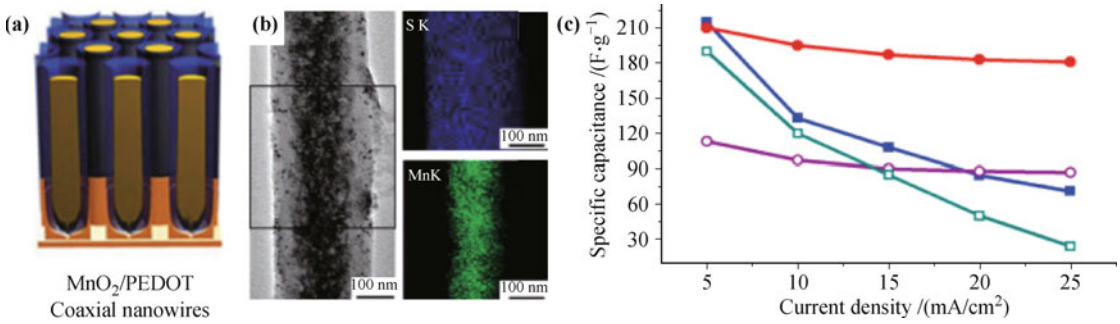

Fig. 6 **(a)** Schematic illustration of MnO_2/PEDOT coaxial nanowires. **(b)** TEM image from a single coaxial nanowire and EDS maps of S and Mn from the boxed area. **(c)** Specific capacitance of MnO_2 nanowires (*closed blue square*), PEDOT nanowires (*open purple dots*), MnO_2 thin film (*open green square*) and MnO_2/PEDOT coaxial nanowires (*closed red dots*) at different charge/discharge current densities. Reproduced from Ref. [69], Copyright © 2008 American Chemical Society.

represent unique, three-dimensional (3D) building blocks for the "bottom-up" paradigm of nanoscience and nanotechnology, with the potential to design novel electronic and electrochemical energy storage nanomaterials and nanodevices. In electrochemical energy storage devices, branched nanowires as electrode can provide more lithium diffusion pathways, enhanced electronic conductivity, better cycling stability and capability due to the synergistic effect of the backbone and branch materials [Fig. 7(a)]. Many branched nanowires have been reported and better electrochemical performance in Li-ion batteries and supercapacitors are achieved [74–81] [Fig. 7(b)–(i)).

Mai *et al.* [82] have synthesized hierarchical $MnMoO_4$/$CoMoO_4$ heterostructured nanowires with enhanced supercapacitor performance. The backbone material $MnMoO_4$ nanowires were prepared by facile micro emulsion method. Hierarchical heterostructures were successfully prepared on the backbone material by a convenient refluxing method under mild conditions. The crystal growth mechanism during the complicated nanoarchitect-ure process is "self-assembly" and "oriented attachment" [Fig. 8(a), (b)]. The specific capacitance and energy density of asymmetric supercapacitors based on

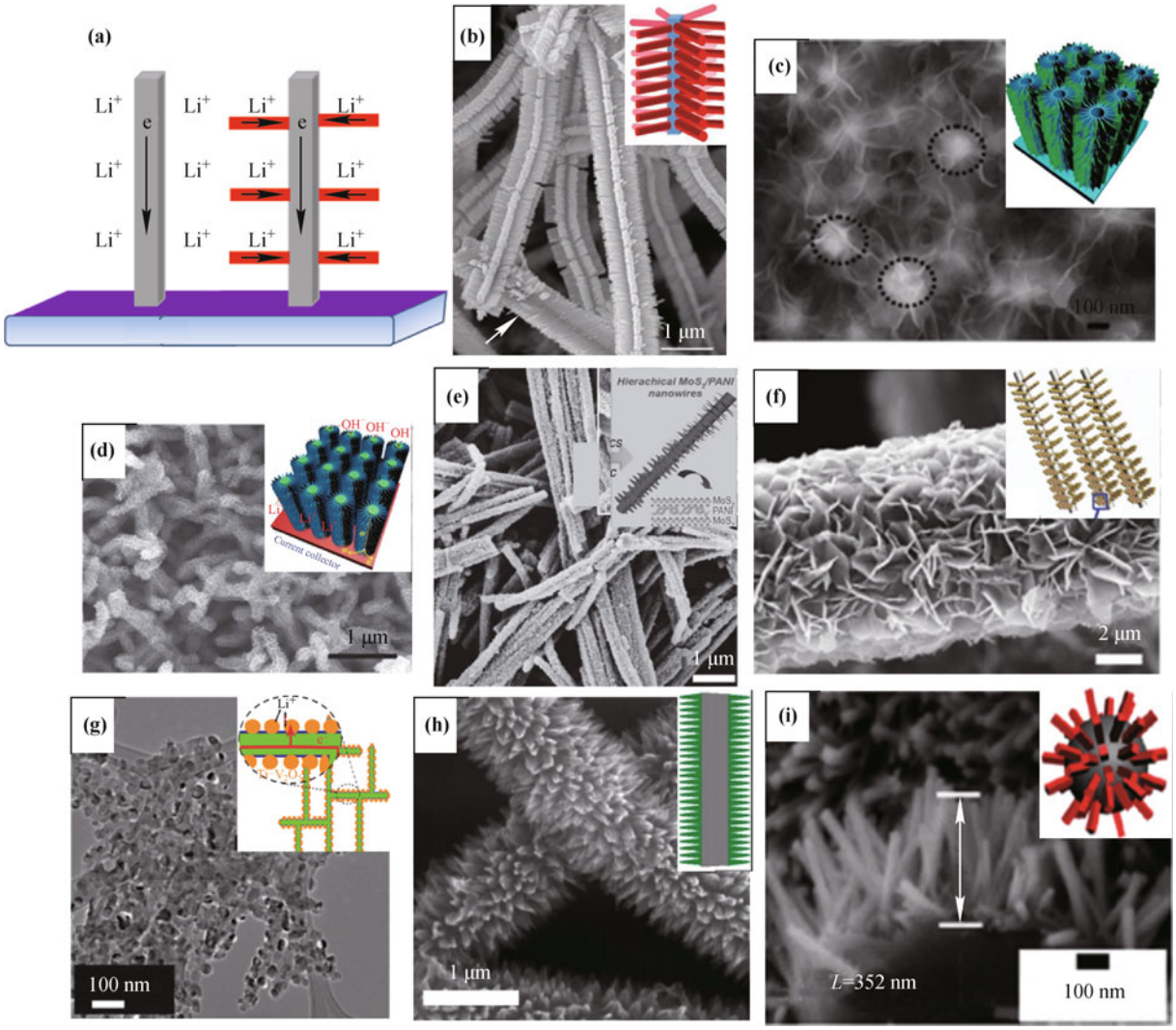

Fig. 7 **(a)** Schematic illustration of lithium ion and electron transport in simple and branched nanowires; **(b)** Typical SEM image of branched nanowires. Reproduced from Ref. [74], Copyright © 2010 Wiley-VCH. **(c)** SEM image of the carbon-coated Co_3O_4@MnO_2 nanowire array after the second 3D interfacial reaction. Reproduced from Ref. [75], Copyright © 2012 Royal Society of Chemistry. **(d)** SEM image of hybrid nanowire arrays. Reproduced from Ref. [76], Copyright © 2011 Wiley-VCH. **(e)** SEM images of MoS_2/PANI-III nanowires. Reproduced from Ref. [77], Copyright © 2012 Wiley-VCH. **(f)** SEM image of the MnO_2 heteronanostructure nanowires. Reproduced from Ref. [78], Copyright © 2012 Royal Society of Chemistry. **(g)** Low magnification TEM image demonstrating the particulate nature of V_2O_5 coating and the interconnectivity of $TiSi_2$ nanowires. Reproduced from Ref. [79], Copyright © 2010 American Chemical Society. **(h)** Top-view SEM image of PANI/GECF. Reproduced from Ref. [80], Copyright © 2012 Royal Society of Chemistry. **(i)** Typical SEM image of nanostructure evolution of SnO_2 nanowire-planted graphite materials. Reproduced from Ref. [81], Copyright © 2011 American Chemical Society.

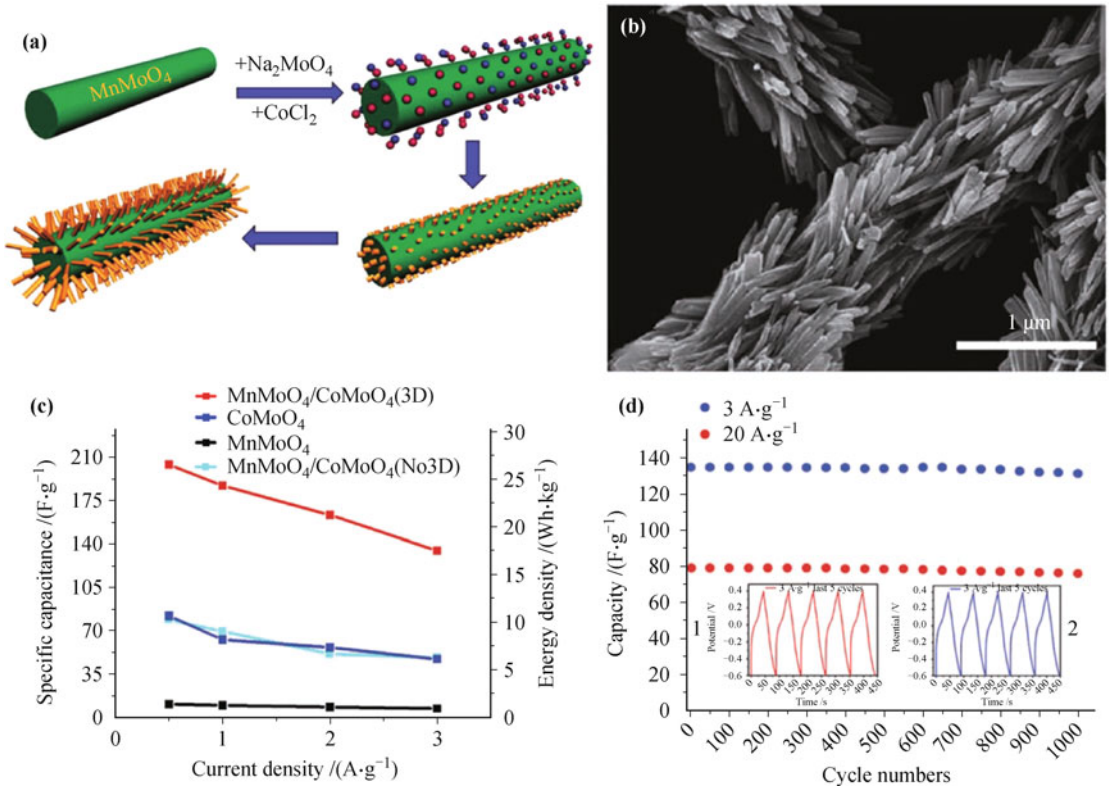

Fig. 8 **(a)** The schematic model diagram of constructing hierarchical $MnMoO_4/CoMoO_4$ heterostructured nanowires. **(b)** SEM images of hierarchical $MnMoO_4/CoMoO_4$ heterostructured nanowires. **(c)** Specific capacitance and energy density of different electrodes at different current densities. **(d)** Charge–discharge cycling of $MnMoO_4/CoMoO_4$ (3D) electrodes at the current density of 3 and 20 A/g performance; inset shows the galvanostatic charge–discharge cyclic curves of the first and last five cycles at 3 A/g. Reproduced from Ref. [82], Copyright © 2011 Nature Publishing Group.

hierarchical $MnMoO_4/CoMoO_4$ heterostructured nanowires, show that the hierarchical $MnMoO_4/CoMoO_4$ electrodes can reach to 204.1, 187.1, 163.4, 134.7 F/g and 28.4, 26.0, 22.7, 18.7 Wh/kg at 0.5, 1, 2, 3 A/g. The capacitance for hierarchical $MnMoO_4/CoMoO_4$ heterostructured nanowires is significantly higher than that for pure one-dimensional nanorods ($MnMoO_4$: 9.7 F/g, 8.8 Wh/kg; $CoMoO_4$: 62.8 F/g, 1.4 Wh/kg; $MnMoO_4/CoMoO_4$ nanocomposite: 69.2 F/g, 9.6 Wh/kg at a charge-discharge current density of 1 A/g), and it shows good reversibility with a cycling efficiency of 98% after 1000 cycles [Fig. 8(c), (d)].

Some similar structures have also been reported. Zhou *et al.* [74] have reported the synthesis of a novel branched nano-heterostructure composed of SnO_2 nanowire stem and α-Fe_2O_3 nanorod branches by combining a vapor transport deposition and a facile hydrothermal method. The length of Fe_2O_3 nanorod branches can be adjusted by tuning the concentration and reacting time of hydrothermal reaction [Fig. 9(a)]. The branched nano-heterostructures show a remarkably improved initial discharge capacity of 1167 mAh/g, which is almost twice the SnO_2 nanowires (612 mAh/g) and α-Fe_2O_3 nanorods (598 mAh/g). Moreover, the composite electrode also exhibits the best initial capacity retention of 69.4%, compared to 56.1% for α-Fe_2O_3 nanorods and 43.6% for SnO_2 nanowires [Fig. 9(b)]. During the charge/discharge process, there exist three main reactions:

$$SnO_2 + 4Li^+ + 4e^- \leftrightarrow Sn + 2Li_2O \quad (1)$$

$$Sn + xLi^+ + xe^- \leftrightarrow Li_xSn (0 \leqslant x \leqslant 4.4) \quad (2)$$

$$Fe_2O_3 + 6Li^+ + 6e^- \leftrightarrow 2Fe + 3Li_2O \quad (3)$$

The equation (3) is fully reversible. Hence, the presence of Fe nanoparticles at the interface between α-Fe_2O_3 and SnO_2 may improve the reversibility of the reaction [Eq. (1)] and further result in a higher reversible capacity. Therefore, branching SnO_2 with a transition metal oxide can be considered as an effective route to resolve the large initial irreversible loss of SnO_2-based anode materials. Besides, the branched α-Fe_2O_3/SnO_2 hierarchical nanowires have significantly large active surface area to incorporate more lithium ions, and this structure can prohibit the structure degradation during cycling, thus improving the cycling stability [Fig. 9(c)].

The branched nanowires can also be as organic–

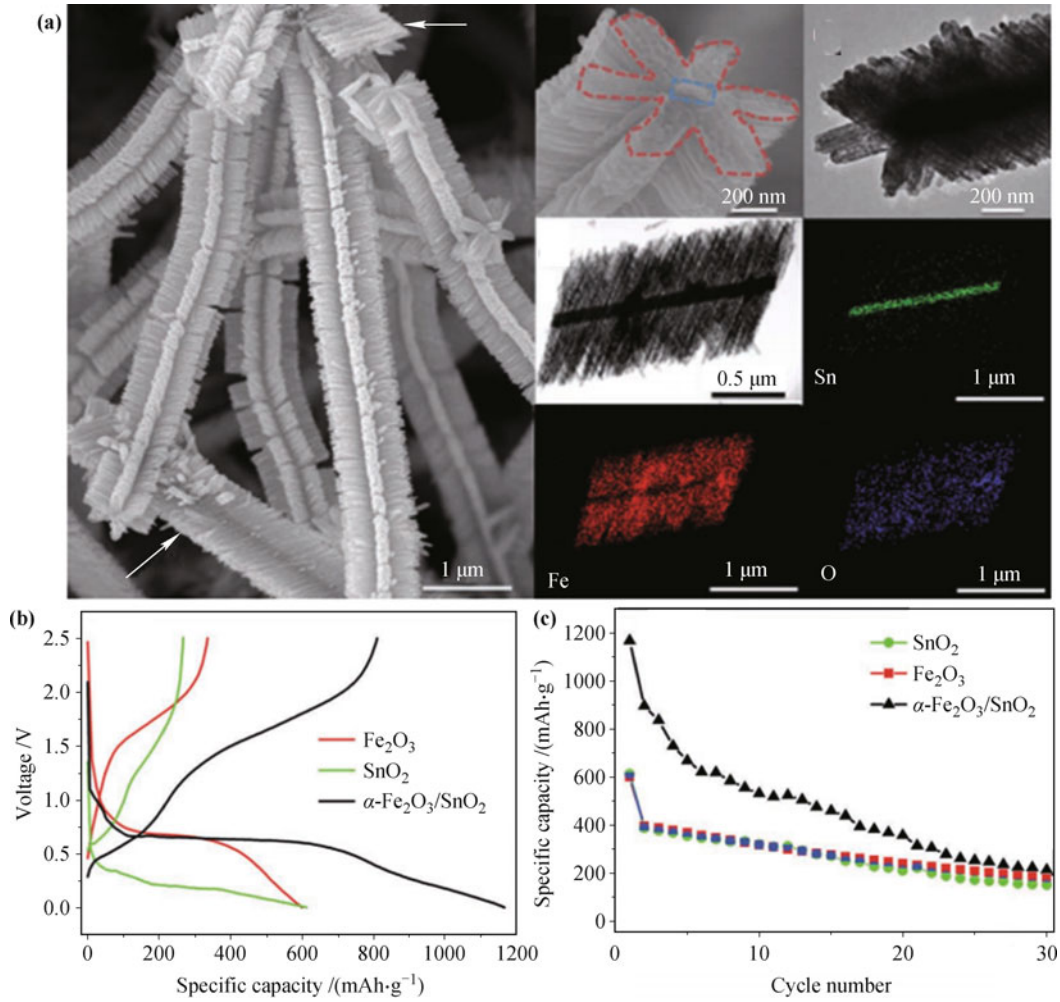

Fig. 9 **(a)** Typical SEM and TEM images of six-fold-symmetry branched nanowires and the corresponding elemental mapping images. **(b)** First charge–discharge profiles at a rate of 1000 mA/g. **(c)** Cycling performance of bare α-Fe_2O_3 nanorod arrays, pristine SnO_2 nanowires, and α-Fe_2O_3/SnO_2 branched nanostructures. Reproduced from Ref. [74], Copyright © 2010 Wiley-VCH.

inorganic composite nanowires. Yang *et al.* [77] have recently reported hierarchical MoS_2/Polyaniline (PANI) nanowires via facile hydrothermal process [Fig. 10(a)]. MoO_x/PANI nanwoires are firstly synthesized after polymerization, and then they are converted to MoS_2/PANI via hydrothermal process with thiourea. The contents of MoS_2 and PANI in nanowires can be easily tuned by adding a varied amount of additional Mo-source. The as-obtained products evenly integrate MoS_2 ultrathin nanosheets with PANI into the primary 1D architecture, resulting in the novel hierarchical and polymer-hybrid nanowires [Fig. 10(b)]. These unique MoS_2/PANI nanowires exhibit greatly improved Li^+ storage properties owing to the hierarchical textures and the PANI-hybrid structures: the charge capacity of 1063.9 mAh/g can be obtained at a current density of 100 mA/g, and retaining 90.2% of the initial reversible capacity after 50 cycles [Fig. 10(c), (d)].

The branched nanowires are more complicated form of exterior design. Combined with coaxial nanowires, both of them can improve the electrochemical performance as they take the advantages of the synergistic effect of the core materials and shell materials.

4 Interiorly designed hierarchical nanowires

To assemble hierarchical nanowires, another strategy is to modify the inner configurations such as component distribution, morphology, concentration, etc. Mesopores, graded components and gradient concentration are examples to achieve the transformation of the nanowires for interior design, which will be elaborated below.

4.1 Substructured nanowires

Herein, substructured nanowires are referred to nano-

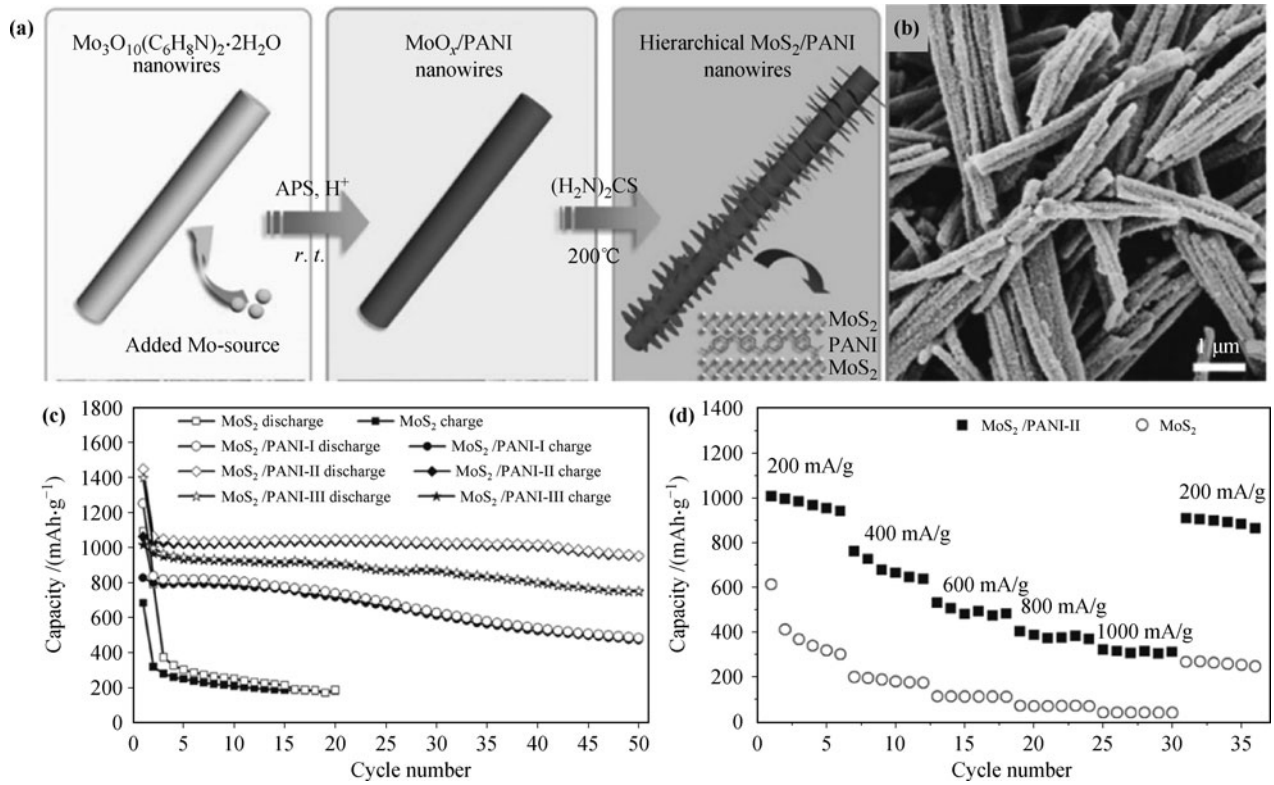

Fig. 10 **(a)** Schematic for the synthesis of hierarchical MoS_2/PANI nanowires through facile polymerization and hydrothermal-treatment of Mo_3O_{10} $(C_6H_8N)_2{\cdot}H_2O$ precursor. **(b)** SEM images of as-synthesized hierarchical MoS_2/PANI nanowires. **(c)** Cycling performance of the MoS_2/PANI nanowires and the commercial MoS_2 microparticles tested in the range of 0.01–3.0 V vs. Li^+/Li at the current density of 100 mA/g. **(d)** Rate performances charge capacity. Reproduced from Ref. [77], Copyright © 2012 Wiley-VCH.

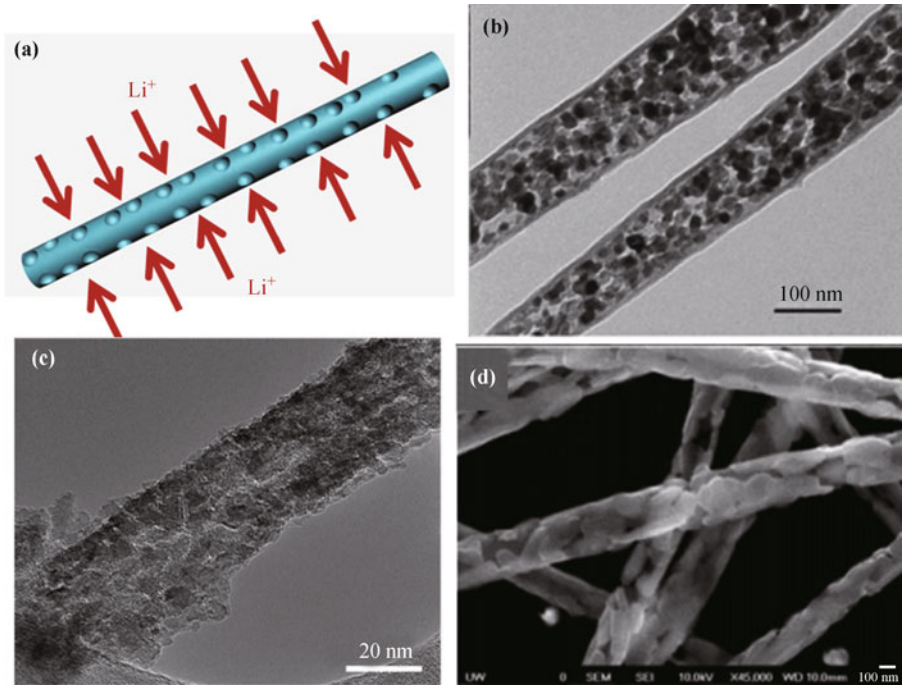

Fig. 11 **(a)** Schematic illustration for mesporous nanowire design. **(b)** TEM image of echinus-like nanostructures of mesoporous CoO nanowire. Reproduced from Ref. [89], Copyright © 2011 Royal Society of Chemistry. **(c)** TEM image of hierarchical porous $NiCo_2O_4$ nanowires. Reproduced from Ref. [90], Copyright © 2012 Royal Society of Chemistry. **(d)** SEM image of mesoporous vanadium pentoxide nanofibers. Reproduced from Ref. [91], Copyright © 2011 Royal Society of Chemistry.

wires which have substructures such as mesopores, micropores or which are composed of many smaller nanorods. It is another kind of hierarchical nanowire as the whole nanowire is interiorly designed and the performance of the nanowire materials is improved.

Mesoporous materials have been widely used in areas such as heterogeneous catalysis, adsorption, separation, gas storage, sensing, etc. [83–88]. They have the advantages such as good access of the electrolyte to the electrode surface, large surface area facilitating charge transfer across the electrode/electrolyte interface, increased utilization of active material and suppressed phase transformations/structure degradations during cycling. This endows mesoporous nanowires many enhanced properties and a promising candidate for energy storage application.

Wu *et al.* [89] have reported amorphous carbon nanotube-encapsulated mesoporous CoO nanorods (CoO@CNT) by a stepwise hydrothermal technique with good control of structure yield, structure uniformity and composite composition and size [Fig. 11(b)]. Porous CoO nanorods (80–150 nm in diameter, 2–5 mm in length) were well confined in amorphous carbon nanotube overlayer (5–10 nm in thickness, 8.5 wt %). Jiang *et al.* [90] have synthesized hierarchical porous $NiCo_2O_4$ nanowires via a facile polyethylene glycol-directed technique at room temperature followed by a suitable thermal treatment [Fig. 11(c)]. Yu *et al.* [91] have fabricated mesoporous V_2O_5 nanofibers with a specific surface area of 97 m^2/g via electrospinning followed by annealing at 500 °C in air [Fig. 11(d)]. The mesoporous nanofibers consist of orthorhombic V_2O_5 with a small amount of residual carbon, and demonstrated a significantly enhanced Li-ion storage capacity of 370 mAh/g, a high charge/discharge rate of up to 800 mA/g, and an excellent cyclic stability and reversibility. Such mesoporous V_2O_5 nanofibers allow easy mass and charge transfer with sufficient freedom for volume change accompanying the lithium ion intercalation and de-intercalation.

Another substructure is defined as a nanowire composed of many attached nanorods, viz. sub-attached nanowires. Mai *et al.* [92] have designed and synthesized ultralong vanadium oxide nanowires with a hierarchical structure by electrospinning combined with annealing [Fig. 12(a)–(c)]. The length of the nanowires can even

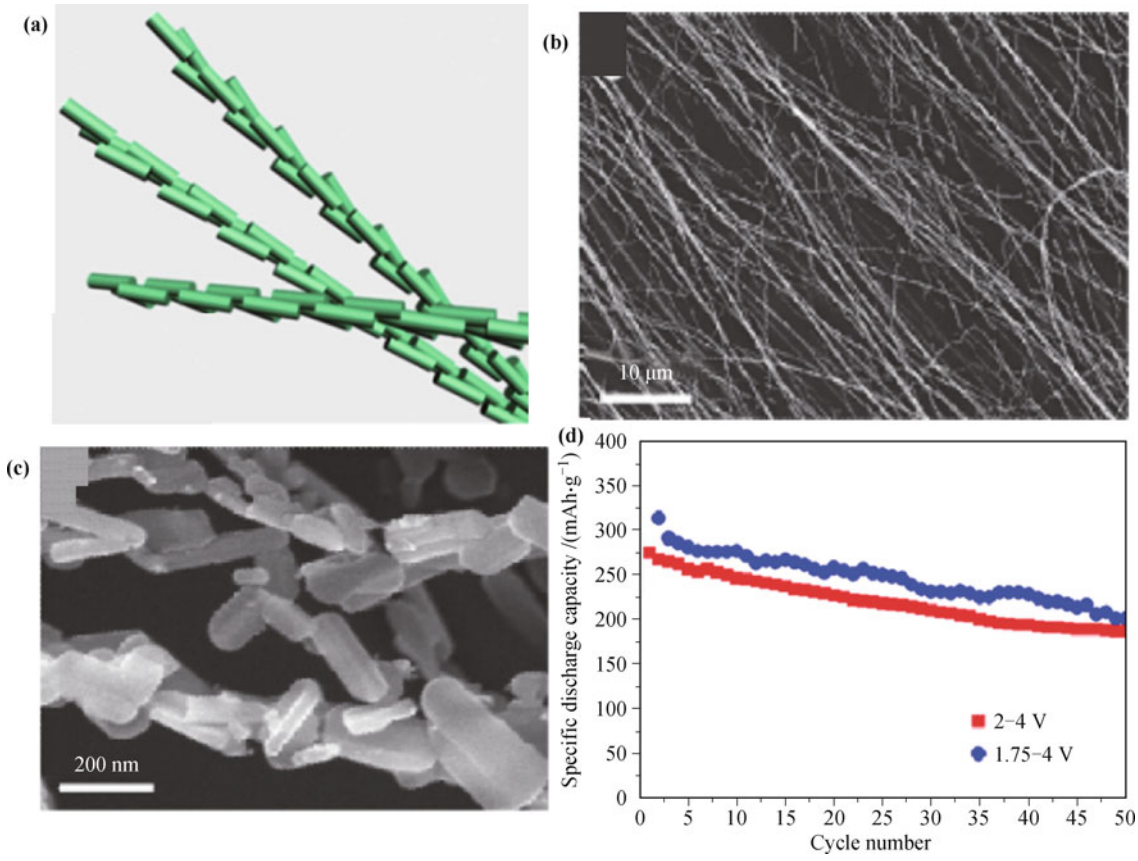

Fig. 12 **(a)** Schematic illustration for the design of the ultralong hierarchical vanadium oxide nanowires. **(b, c)** SEM images of the ultralong hierarchical vanadium oxide nanowires. **(d)** Capacity vs. cycle number of the ultralong hierarchical vanadium oxide nanowires. Reproduced from Ref. [92], Copyright © 2010 American Chemical Society.

reach the millimeter or centimeter scale, and notably, the ultralong vanadium oxide nanowires were constructed from attached nanorods of diameter around 50 nm and length of 100 nm. The initial and 50th discharge capacities of the ultralong hierarchical vanadium oxide nanowire cathodes are up to 390 mAh/g and 201 mAh/g when the lithium battery cycled between 1.75 and 4.0 V. When the battery was cycled between 2.0 and 4.0 V, the initial and 50th discharge capacities of the nanowire cathodes are 275 mAh/g and 187 mAh/g, which is much higher than self-aggregated short nanorods with a discharge capacity of 110–130 mAh/g [Fig. 12(d)]. This is due to the fact that self-aggregation of the unique nanorod-in-nanowire structures have been greatly reduced because of the attachment of nanorods in the ultralong nanowires, which can keep the effective contact areas of active materials, conductive additives and electrolyte large and maximize the superiority of nanomaterial-based cathodes.

Combined with the above two substructured nanowires of mesoporous nanowires and sub-attached nanowires, Zhao *et al.* [93] have synthesized hierarchical mesoporous perovskite $L_{a0.5}Sr_{0.5}CoO_{2.91}$(LSCO) nanowires. LSCO nanorods first crystallize and grow in the micro-emulsion of $La(NO_3)_3$, $Sr(NO_3)_2$, $Co(NO_3)_2$, and KOH at a high stirring rate. Then LSCO nanorods self-assemble at a low stirring rate and a bigger water pool in micro-emulsion, and then LSCO nanorods play the role of a template itself for the oriented growth of attached nanorods, which results in the formation of hierarchical mesoporous LSCO nanowires [Fig. 13(a)]. LSCO nanorods are tightly attached to each other at an atomic level when they formed the hierarchical nanowire, which provides good physical contact between the nanorods and an increased oxygen pathway and is beneficial for electronic conduction [Fig. 13(b)]. The specific capacity of the Li-air battery based on hierarchical mesoporous LSCO nanowires is over 11 000 mAh/g, which exhibits ultrahigh performance for the Li-air battery [Fig. 13(c)].

4.2 Graded/gradient nanowires

Hierarchical nanomaterials have some advantages over simple-structured nanomaterials; however, the interface between different component materials has always caused some problems, especially if there is a sharp variation of the composition at this point. Based on this view of point, strain-graded nanomatierials and concentration-gradient nanomaterials have been developed and synthesized to fully optimize the interface

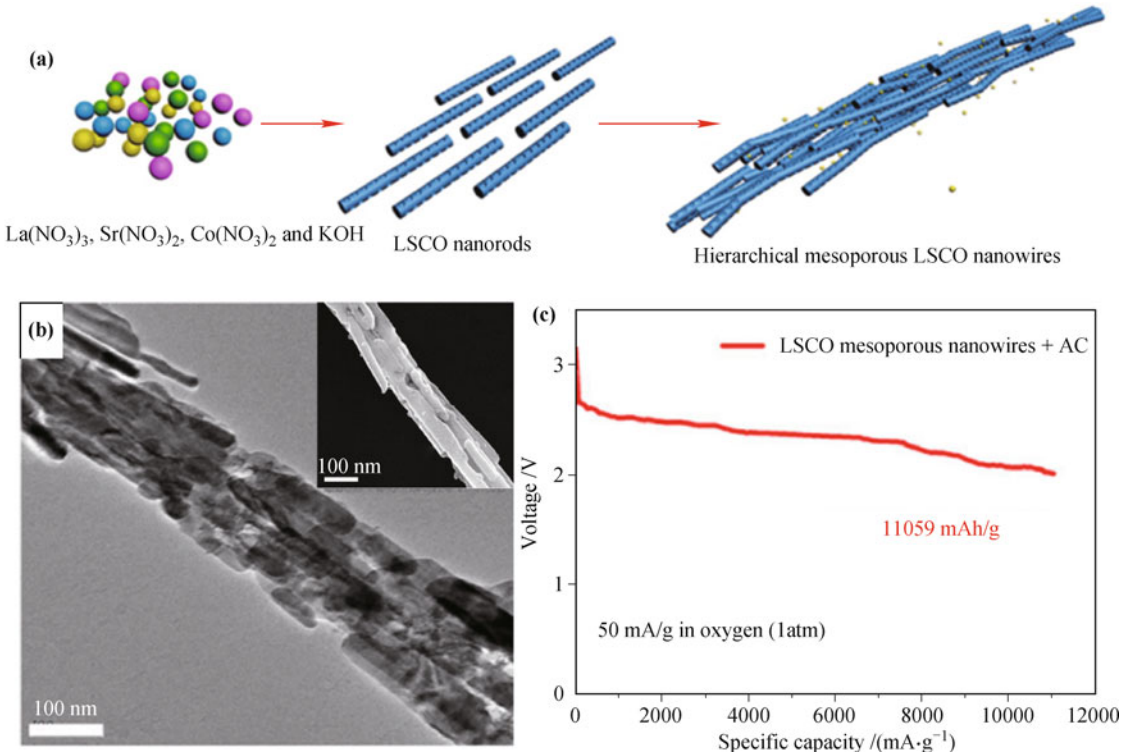

Fig. 13 **(a)** The schematic model diagram of constructing hierarchical mesoporous LSCO nano wires. **(b)** TEM and SEM (inset) images of the hierarchical mesoporous LSCO nanowires. **(c)** The discharge curve of Li-air batteries using hierarchical mesoporous LSCO nanowires + acetylene carbon as the air electrode in oxygen (P_{O_2} = 1 atm). Reproduced from Ref. [93], Copyright © 2012 Proceedings of the National Academy of Sciences.

mismatch and enhance the performance.

Sun *et al.* [94–96] have developed series of concentration-gradient nickel-rich layered lithium transition-metal oxides nanoparticles by co-precipitation method. Gradients in the internal core composition, external shell composition and full-gradient from the centre to the outer layer of the particles were achieved and monitored. Compared with the bulk composition $Li(Ni_{0.8}Co_{0.1}Mn_{0.1})O_2$, the concentration-gradient material showed superior performance in electrochemical performance. Though this work focused on particles with a micrometer scale, such a concentration-gradient design could be extended to nanowire materials and a favorable result could be predicted.

Another potential optimization strategy for interface issue lays in hierarchical structure construction, where a buffer layer can be added between two component materials which are endowed with different Li uptake capacities and hence vast differences in volumetric strains during cycling. For example, silicon-carbon composites, which have often been studied as anode materials, have suffered from great mismatch at the interfaces between C and Si during cycling, resulting in poor performance at fast C-rates. In terms of this, Rahul *et al.* [97] reported a functionally strain-graded C-Al-Si anode architecture, where the intermediate material Al helps to gradually transit the strain from the least strained material of C to the most strained material of Si [Fig. 14(a), (b)]. Such a strain-graded nanoarchitecture could efficiently uptake lithium even under extremely rapid rates (~51.2 A/g), providing average capacities of ~412 mAh/g with a power output of ~100 kW/kg continuously over 100 cycles [Fig. 14(c)].

The concentration-gradient or graded nanowires are relatively less reported for the difficulty in controllable synthesis; however they are promising candidates for solving the many problems and breaking the limitations in nanowires for electrochemical energy storage.

5 Aligned nanowires

Organizing the nanoscale building blocks into hierarchical ordered nanowire architectures, where nanowires are vertically or horizontally aligned on conductive substrates, offers another way to overcome the self-aggregation issue. As each nanowire is fixed in a certain position and separated from each other, such architecture brings several advantages. First, the detached state of nanowires can greatly avoid self-aggregation, and free space between them could promote facile strain relaxation during battery operation. Second, nanowires are attached to the current collector for good adhesion and form continuous conducting pathways for electrons, which makes the binders and conducting additives unnecessary. Third, ordered nanowire architectures, compared with nanowires with disordered form, have bigger specific surface area and lower average concentration of structural defects and grain boundaries, resulting in increased Li^+ insertion/extraction rate and electron transport [98, 99] [Fig. 15(a)].

Aligned nanowires have been synthesized and assembled by various synthesis methods and have been widely applied in energy storage systems. Meduri *et al.* [100]

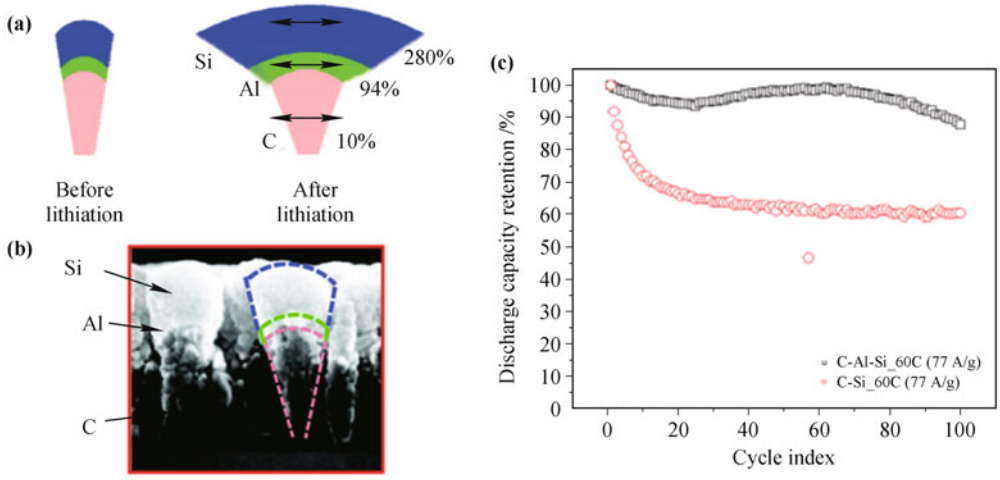

Fig. 14 **(a)** Illustration of the principle of strain-graded multilayer nanostructures. **(b)** Cross-section SEM image of C-Al-Si nanoscoop structures deposited on a Si wafer with the C, Al, and Si regions demarcated. **(c)** Comparison at ~51.2 A/g current density of the charge/discharge capacity versus cycle number for the C-Al-Si electrode versus an electrode comprised of only C nanorods. The length and diameter of the C nanorods in the control sample are identical to those of the C nanorods in the C-Al-Si multilayer structure. Reproduced from Ref. [97], Copyright © 2010 American Chemical Society.

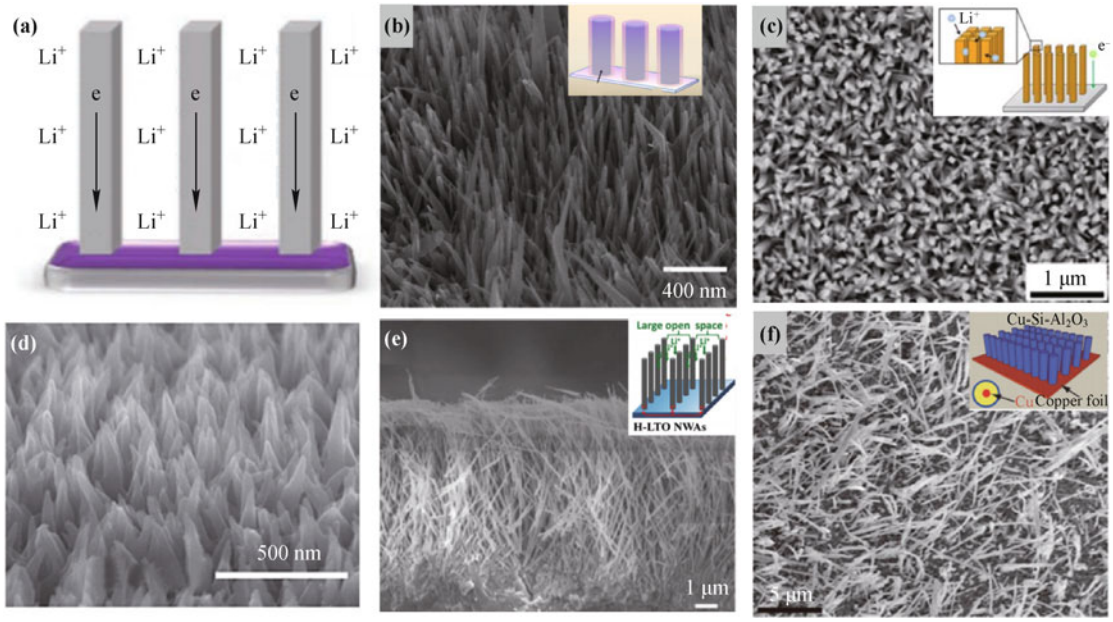

Fig. 15 **(a)** Schematic illustration of aligned nanowires for improving lithium ion diffusion and electron transport. **(b)** SEM image of MoO_{3-x} nanowire arrays. Reproduced from Ref. [100], Copyright © 2012 American Chemical Society. **(c)** SEM image of aligned mesocrystalline SnO_2 nanowire Arrays. Reproduced from Ref. [101], Copyright © 2013 Royal Society of Chemistry. **(d)** SEM images of two-ply yarn supercapacitors based on carbon nanotubes and polyaniline nanowire arrays. Reproduced from Ref. [102], Copyright © 2013 Wiley-VCH. **(e)** SEM image of hydrogenated $Li_4Ti_5O_{12}$ nanowire arrays. Reproduced from Ref. [103], Copyright © 2012 Wiley-VCH. **(f)** SEM images of Cu-Si nanocable arrays. Reproduced from Ref. [104], Copyright © 2011 Wiley-VCH.

have reported a chemical vapor deposition method to grow MoO_{3-x} nanowire arrays on metallic substrates with diameters of ~90 nm, and the nanowires show high capacity retention [Fig. 15(b)]. Chen *et al.* [101] have developed a general method for facile kinetics controlled growth of aligned arrays of mesocrystallline SnO_2 nanorods on arbitary substrates by adjusting supersaturation in a unique ternary solvent system [Fig. 15(c)]. Wang *et al.* [102] constructed thread-like supercapacitors from two-ply CNT and PANI composite yarns using a simple process. The resultant supercapacitor, which is finer than a conventional fine count cotton yarn, takes the form of a two-ply composite yarn consisting of two carbon nanotube (CNT) singles yarns that are infiltrated with polyaniline nanowire arrays [Fig. 15(d)]. Shen *et al.* [103] have fabricated self-supported $Li_4Ti_5O_{12}$ (LTO) nanowire arrays architectures on Ti foil by a facile solution chemical approach and enhance its electronic conductivity by creating Ti^{3+} sites through hydrogenation [Fig. 15(e)]. Creating surface defects is a very simple yet very effective approach to enhancing ion or/and electron conductivity, it may also be extended to other anode and anode materials. The Ti^{3+} groups on the surface of the electrode could enhance the nanowire conductivity and the high electrical conductivity of H-LTO NWAs as compared with pristine LTO NWAs results in their high capacity, excellent rate capability and good cyclic stability. Cao *et al.* [104] reported a new concept of using Cu-Si nanocable arrays directly anchored on a current collector to promote both the cycling stability and the high rate capability of Si as an anode of LIBs [Fig. 15(f)]. Here, the conductive Cu core was grown from the current collector forming a 3D current collector substrate, which allows for effective electron conduction to enhance the battery's high rate performance. Besides, the robust Cu core provides structural reinforcement to overcome the mechanical rupture during the volume changes of Si. Furthermore, the space between the nanocables can accommodate large Si expansion and an additional coating with, e.g., Al_2O_3, could stabilize the Si/electrolyte interface and trigger a stable SEI formation for long cycle lifetime. The Cu-Si-Al_2O_3 nanocables exhibit even higher specific capacities, especially under high discharge and charge currents.

Alighed nanowires can be divided into two categories, i.e., vertically aligned arrays and horizontally aligned arrays. Mai *et al.* [105] have also reported a substrate-assisted hydrothermal method in synthesizing moundlily like aligned β-$AgVO_3$ nanowire clusters [Fig. 16(a), (b)]. Gravitation and F^- ions have been demonstrated to play important roles in the growth of β-$AgVO_3$ nanowires (NWs) on substrates. The moundlily like β-$AgVO_3$ nanowire cathode has a high discharge capacity and excellent cycling performance, mainly due to the reduced

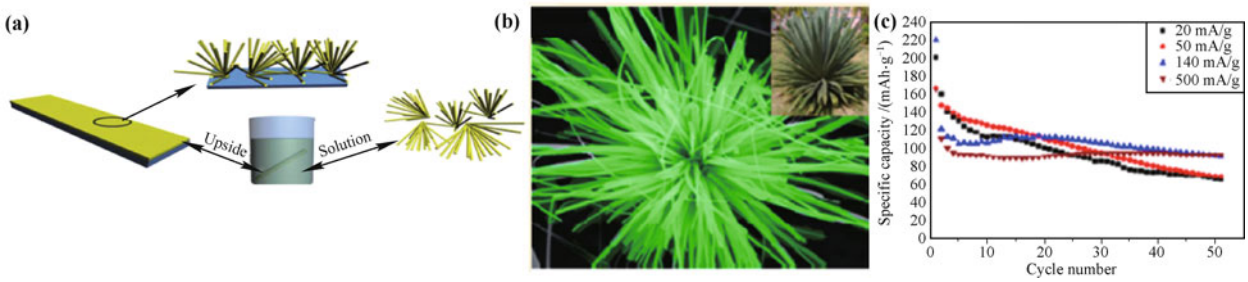

Fig. 16 **(a)** Schematic mechanism for the growth process of one-dimensional β-$AgVO_3$ grown on the up side of substrate; **(b)** SEM images of radial β-$AgVO_3$ grown on the ITO substrate, the real moundlily shown in the inset; **(c)** Capacity vs. cycle number of β-$AgVO_3$ nanowire array cathode at different current densities. Reproduced from Ref. [105], Copyright © 2012 American Chemical Society.

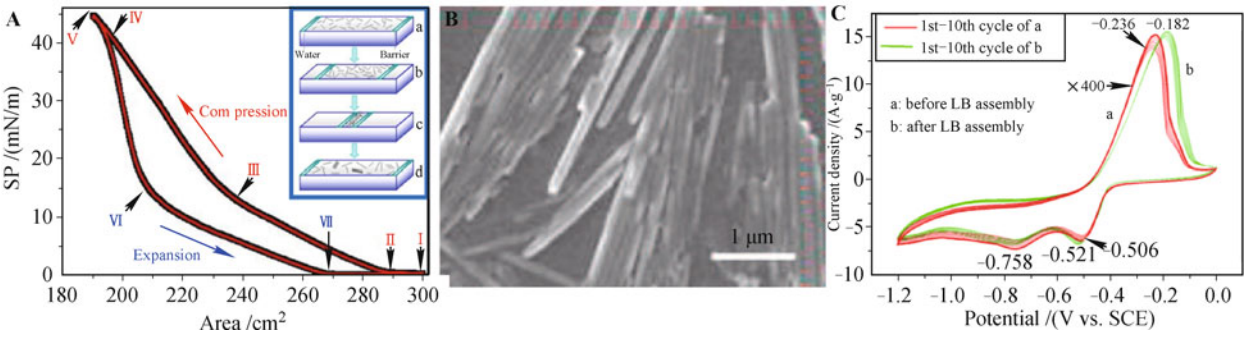

Fig. 17 **(A)** π-*A*isotherm of VO_2 nanowires floating on the water during compression and expansion cycle. *Inset*: schematic illustration of the behavior of nanowires during compression and expansion cycle. (a) Nanowire units floating on water after dispersion are fairly monodispersed with no superstructures, and the directions of the nanowires are isotropically distributed. (b) Wires with uniform size and small aspect ratio form raftlike aggregates of generally three to five wires by aligning side-by-side after compression. (c) With further compression the nanowires isotropically distributed align with their long axis at local areas. (d) Raftlike aggregates remained after relaxation. **(B)** Typical SEM images of VO_2 nanowire LB films assembled at surface pressure of 15 mN/m. **(C)** CV graphs of VO_2 aligned nanowire film before and after the LB assembly. Reproduced from Ref. [106], Copyright © 2009 American Chemical Society.

self-aggregation. The capacity fading per cycle from 3rd to 51st is 0.17% under the current density of 500 mA/g [Fig. 16(c)]. This method is shown to be an effective and facile technique for improving the electrochemical performance for applications in rechargeable Li batteries or Li-ion batteries.

As for horizontally aligned nanowires, Mai *et al.* [106] have reported Langmuir–Blodgett (LB) based assembly of vanadium dioxide (VO_2) nanowires. VO_2 nanowires were functionalized with stearic acid (SA) and cetyltrimethylammonium bromide (CTAB) and then spread on the surface in an aqueous phase in a LB trough. Figure 17(A) is schematic illustration provides schematic explanation for the observed hysteretic π-*A* data recorded during compression and expansion at different surface pressures. Different parts of the curve corresponding to different states of the film. When the nanowires are compressed with increasing surface pressure, the nanowire with uniform size and small aspect ratio approach each other at smaller area and form raftlike aggregates; the raftlike aggregates approach each other and the nanowires are aligned locally. The uniform sized nanowires will form raftlike aggregates by aligning side-by-side due to the directional capillary force and the van der Waals attraction [Fig. 17(B)]. Surface pressure-area (π-*A*) isotherms were recorded on the LB trough and show hysteretic behavior. At zero surface pressure, the nanowires are monodispersed on the trough's water surface with an isotropical distribution. And the results show that the current density and specific capacity are enhanced by ~2 orders after LB assembly by cyclic voltammetry [Fig. 17(C)], and the conductivity also increase 2 orders of magnitude. Comparing to the nanowire film and gel film, the improvement in efficiency can be obviously observed.

Aligned nanowires have the advantages of high order and facility for large scale production, and the substrates could be adjusted to various applications, hence giving aligned nanowires great potential in the future development for hierarchical nanowires.

6 Conclusion and prospect

In this review, we have summarized the effective ways to enhance the electrochemical performance of nanowires via assembling hierarchical nanowire structures, including exterior assembly design of coaxial nanowires and branched nanowires, interior design of graded nanowires and substructured nanowires. The design of both integrating interior and exterior to fabricate future hierarchical nanowires in the application of energy storage is also discussed and prospected.

For the future development for hierarchical nanowires, combining the interior design, exterior design and aligned nanowire assembly is a valuable method and solution, i.e., core-shell mesoporous nanowires, concentration-degraded nanowire arrays, etc. The improvements in exterior and interior of nanowires will endow nanowires better performance as a result of the synergistic advantages. This method is promising and applicable in other energy storage applications based on nanowires materials. Besides, some other novel hierarchical nanowires such as nanosheet-intercalated nanowires, beads-like nanowires and nanowires blocks with aligned mesopores should be explored in energy storage systems. Simultaneously, the theories and mechanisms of hierarchical nanowire synthesis, assembly and performance needs to be further explored.

Acknowledgements This work was supported by the National Basic Research Program of China (Grant Nos. 2013CB934103 and 2012CB933003), the National Natural Science Foundation of China (Grant Nos. 51272197 and 51072153), the Program for New Century Excellent Talents in University (Grant No. NCET-10-0661), the International Science and Technology Cooperation (Grant No. 2013DFA50840), and the Fundamental Research Funds for the Central Universities (Grant Nos. 2012-Ia-011 and 2013-VII-028). We express our deep thanks to Professor C. M. Lieber of Harvard University, Professor D. Y. Zhao of Fudan University, Professor Z. L. Wang of Georgia Institute of Technology, Professor Q. J. Zhang of Wuhan University of Technology, and Dr. Y. J. Dong of QD Vision, Inc. for fruitful collaboration and stimulating discussion.

References

1. M. Armand and J. M. Tarascon, Building better batteries, *Nature*, 2008, 451(7179): 652
2. D. R. Rolison and L. F. Nazar, Electrochemical energy storage to power the 21st century, *MRS Bull.*, 2011, 36(07): 486
3. S. Chu and A. Majumdar, Opportunities and challenges for a sustainable energy future, *Nature*, 2012, 488(7411): 294
4. B. Scrosati and J. Garche, Lithium batteries: Status, prospects and future, *J. Power Sources*, 2010, 195(9): 2419
5. M. M. Thackeray, C. Wolverton, and E. D. Isaacs, Electrical energy storage for transportation-approaching the limits of, and going beyond, lithium-ion batteries, *Energy Environ. Sci.*, 2012, 5(7): 7854
6. J. Liu, Addressing the grand challenges in energy storage, *Adv. Funct. Mater.*, 2013, 23(8): 924
7. L. Su, Y. Jing, and Z. Zhou, Li ion battery materials with core-shell nanostructures, *Nanoscale*, 2011, 3(10): 3967
8. T. Nagaura and K. Tozawa, Lithium ion rechargeable battery, *Progress in Batteries and Solar Cells*, 1990, 9: 209
9. B. Dunn, H. Kamath, and J. M. Tarascon, Electrical energy storage for the grid: A battery of choices, *Science*, 2011, 334(6058): 928
10. P. G. Bruce, S. A. Freunberger, L. J. Hardwick, and J. M. Tarascon, Li-O_2 and Li-S batteries with high energy storage, *Nat. Mater.*, 2012, 11(1): 19
11. C. Bai and M. Liu, From chemistry to nanoscience: Not just a matter of size, *Angew. Chem. Int. Ed.*, 2013, 52(10): 2678
12. P. G. Bruce, B. Scrosati, and J. M. Tarascon, Nanomaterials for rechargeable lithium batteries, *Angew. Chem. Int. Ed.*, 2008, 47(16): 2930
13. J. Thomas, Lithium batteries: A spectacularly reactive cathode, *Nat. Mater.*, 2003, 2(11): 705
14. A. S. Aricò, P. Bruce, B. Scrosati, J. M. Tarascon, and W. van Schalkwijk, Nanostructured materials for advanced energy conversion and storage devices, *Nat. Mater.*, 2005, 4(5): 366
15. J. B. Goodenough, Cathode materials: A personal perspective, *J. Power Sources*, 2007, 174(2): 996
16. L. Q. Mai, F. Yang, Y. L. Zhao, X. Xu, L. Xu, B. Hu, Y. Z. Luo, and H. Y. Liu, Molybdenum oxide nanowires: Synthesis & properties, *Mater. Today*, 2011, 14(7–8): 346
17. M. Hu, X. Pang, and Z. Zhou, Recent progress in high-voltage lithium ion batteries, *J. Power Sources*, 2013, 237: 229
18. C. M. Lieber, One-dimensional nanostructures: Chemistry, physics & applications, *Solid State Commun.*, 1998, 107(11): 607
19. Y. Xia, P. Yang, Y. Sun, Y. Wu, B. Mayers, B. Gates, Y. Yin, F. Kim, and H. Yan, One-dimensional nanostructures: Synthesis, characterization, and applications, *Adv. Mater.*, 2003, 15(5): 353
20. A. I. Hochbaum and P. Yang, Semiconductor nanowires for energy conversion, *Chem. Rev.*, 2010, 110(1): 527
21. X. Duan and C. M. Lieber, General synthesis of compound semiconductor nanowires, *Adv. Mater.*, 2000, 12(4): 298
22. P. Yang, R. Yan, and M. Fardy, Semiconductor nanowire: What's next? *Nano Lett.*, 2010, 10(5): 1529
23. T. J. Kempa, R. W. Day, S.K. Kim, H.G. Park, and C. M. Lieber, Semiconductor nanowires: A platform for exploring limits and concepts for nano-enabled solar cells, *Energy Environ. Sci.*, 2013, 6(3): 719
24. J.-M. Tarascon and M. Armand, Issues and challenges facing rechargeable lithium batteries, *Nature*, 2001, 414(6861): 359

25. L. Q. Mai, B. Hu, W. Chen, Y. Y. Qi, C. Lao, R. Yang, Y. Dai, and Z. L. Wang, Lithiated MoO_3 nanobelts with greatly improved performance for lithium batteries, *Adv. Mater.*, 2007, 19(21): 3712
26. X. H. Liu, J. W. Wang, S. Huang, F. Fan, X. Huang, Y. Liu, S. Krylyuk, J. Yoo, S. A. Dayeh, A. V. Davydov, S. X. Mao, S. T. Picraux, S. Zhang, J. Li, T. Zhu, and J. Y. Huang, In situ atomic-scale imaging of electrochemical lithiation in silicon, *Nat. Nanotechnol.*, 2012, 7(11): 749
27. M. T. McDowell, I. Ryu, S. W. Lee, C. Wang, W. D. Nix, and Y. Cui, Studying the kinetics of crystalline silicon nanoparticle lithiation with in situ transmission electron microscopy, *Adv. Mater.*, 2012, 24(45): 6034
28. R. Ruffo, S. S. Hong, C. K. Chan, R. A. Huggins, and Y. Cui, Impedance analysis of silicon nanowire lithium ion battery anodes, *J. Phys. Chem. C*, 2009, 113(26): 11390
29. A. R. Armstrong, C. Lyness, P. M. Panchmatia, M. S. Islam, and P. G. Bruce, The lithium intercalation process in the low-voltage lithium battery anode $Li_{1+x}V_{1-x}O_2$, *Nat. Mater.*, 2011, 10(3): 223
30. M. Pharr, K. Zhao, X. Wang, Z. Suo, and J. J. Vlassak, Kinetics of initial lithiation of crystalline silicon electrodes of lithium-ion batteries, *Nano Lett.*, 2012, 12(9): 5039
31. Y. Yang, C. Xie, R. Ruffo, H. Peng, K. Kim, and Y. Cui, Single nanorod devices for battery diagnostics: A case study on $LiMn_2O_4$, *Nano Lett.*, 2009, 9(12): 4109
32. L. Q. Mai, Y. J. Dong, L. Xu, and C. H. Han, Single nanowire electrochemical devices, *Nano Lett.*, 2010, 10(10): 4273
33. J. Y. Huang, L. Zhong, C. M. Wang, J. P. Sullivan, W. Xu, L. Q. Zhang, S. X. Mao, N. S. Hudak, X. H. Liu, A. Subramanian, H. Fan, L. Qi, A. Kushima, and J. Li, In situ observation of the electrochemical lithiation of a single SnO_2 nanowire electrode, *Science*, 2010, 330(6010): 1515
34. R. Liu, J. Duay, and S. B. Lee, Heterogeneous nanostructured electrode materials for electrochemical energy storage, *Chem. Commun.*, 2010, 47(5): 1384
35. X. Liu, Y. Lin, S. Zhou, S. Sheehan, and D. Wang, Complex nanostructures: Synthesis and energetic applications, *Energies*, 2010, 3(3): 285
36. C. Cheng and H. J. Fan, Branched nanowires: Synthesis and energy applications, *Nano Today*, 2012, 7(4): 327
37. H. Li, A. G. Kanaras, and L. Manna, Colloidal branched semiconductor nanocrystals: State of the art and perspectives, *Acc. Chem. Res.*, 2013, doi:10.1021/ar3002409
38. S. K. Kim, R. W. Day, J. F. Cahoon, T. J. Kempa, K. D. Song, H. G. Park, and C. M. Lieber, Tuning light absorption in core/shell silicon nanowire photovoltaic devices through morphological design, *Nano Lett.*, 2012, 12(9): 4971
39. J. Tang, Z. Huo, S. Brittman, H. Gao, and P. Yang, Solution-processed core-shell nanowires for efficient photovoltaic cells, *Nat. Nanotechnol.*, 2011, 6(9): 568
40. B. Tian, T. J. Kempa, and C. M. Lieber, Single nanowire photovoltaics, *Chem. Soc. Rev.*, 2009, 38(1): 16
41. Y. J. Hwang, C. H. Wu, C. Hahn, H. E. Jeong, and P. Yang, Si/InGaN core/shell hierarchical nanowire arrays and their photoelectrochemical properties, *Nano Lett.*, 2012, 12(3): 1678
42. Y. J. Hwang, A. Boukai, and P. D. Yang, High density n-Si/n-TiO_2 core/shell nanowire arrays with enhanced photoactivity, *Nano Lett.*, 2009, 9(1): 410
43. C. Pan, S. Niu, Y. Ding, L. Dong, R. Yu, Y. Liu, G. Zhu, and Z. L. Wang, Enhanced Cu_2S/CdS coaxial nanowire solar cells by piezo-phototronic effect, *Nano Lett.*, 2012, 12(6): 3302
44. Y. Dong, B. Tian, T. J. Kempa, and C. M. Lieber, Coaxial group III-nitride nanowire photovoltaics, *Nano Lett.*, 2009, 9(5): 2183
45. F. Zhang, Y. Ding, Y. Zhang, X. Zhang, and Z. L. Wang, Piezo-phototronic effect enhanced visible and ultraviolet photodetection using a ZnO-CdS core-shell micro/nanowire, *ACS Nano*, 2012, 6(10): 9229
46. T. J. Kempa, J. F. Cahoon, S. K. Kim, R. W. Day, D. C. Bell, H. G. Park, and C. M. Lieber, Coaxial multishell nanowires with high-quality electronic interfaces and tunable optical cavities for ultrathin photovoltaics, *Proc. Natl. Acad. Sci. USA*, 2012, 109(5): 1407
47. B. Z. Tian and C. M. Lieber, Design, synthesis, and characterization of novel nanowire structures for photovoltaics and intracellular probes, *Pure Appl. Chem.*, 2011, 83(12): 2153
48. Y. Hu, J. Xiang, G. Liang, H. Yan, and C. M. Lieber, Sub-100 nanometer channel length Ge/Si nanowire transistors with potential for 2 THz switching speed, *Nano Lett.*, 2008, 8(3): 925
49. Q. Yang, Y. Liu, C. Pan, J. Chen, X. Wen, and Z. L. Wang, Largely enhanced efficiency in ZnO nanowire/p-polymer hybridized inorganic/organic ultraviolet light-emitting diode by piezo-phototronic effect, *Nano Lett.*, 2013, 13(2): 607
50. H. Peng, C. Xie, D. T. Schoen, K. McIlwrath, X. F. Zhang, and Y. Cui, Ordered vacancy compounds and nanotube formation in $CuInSe_2$-CdS coreshell nanowires, *Nano Lett.*, 2007, 7(12): 3734
51. G. Liang, J. Xiang, N. Kharche, G. Klimeck, C. M. Lieber, and M. Lundstrom, Performance analysis of a Ge/Si core/shell nanowire field-effect transistor, *Nano Lett.*, 2007, 7(3): 642
52. L. J. Lauhon, M. S. Gudiksen, D. Wang, and C. M. Lieber, Epitaxial core-shell and core-multishell nanowire heterostructures, *Nature*, 2002, 420(6911): 57
53. Y. Hu, F. Kuemmeth, C. M. Lieber, and C. M. Marcus, Hole spin relaxation in Ge-Si core-shell nanowire qubits, *Nat. Nanotechnol.*, 2012, 7(1): 47
54. B. Tian, X. Zheng, T. J. Kempa, Y. Fang, N. Yu, G. Yu, J. Huang, and C. M. Lieber, Coaxial silicon nanowires as solar cells and nanoelectronic power sources, *Nature*, 2007, 449(7164): 885
55. Y. Dong, G. Yu, M. C. McAlpine, W. Lu, and C. M. Lieber,

Si/a-Si core/shell nanowires as nonvolatile crossbar switches, *Nano Lett.*, 2008, 8(2): 386

56. Y. Hu, H. O. Churchill, D. J. Reilly, J. Xiang, C. M. Lieber, and C. M. Marcus, A Ge/Si heterostructure nanowire-based double quantum dot with integrated charge sensor, *Nat. Nanotechnol.*, 2007, 2(10): 622
57. T. Mokari, S. E. Habas, M. Zhang, and P. Yang, Synthesis of lead chalcogenide alloy and core-shell nanowires, *Angew. Chem. Int. Ed.*, 2008, 47(30): 5605
58. C. R. Ghosh and S. Paria, Core/shell nanoparticles: Classes, properties, synthesis mechanisms, characterization, and applications, *Chem. Rev.*, 2012, 112(4): 2373
59. S. Wei, Q. Wang, J. Zhu, L. Sun, H. Lin, and Z. Guo, Multifunctional composite core-shell nanoparticles, *Nanoscale*, 2011, 3(11): 4474
60. W. M. Zhang, X. L. Wu, J. S. Hu, Y. G. Guo, and L. J. Wan, Carbon coated Fe_3O_4 nanospindles as a superior anode material for lithium-ion batteries, *Adv. Funct. Mater.*, 2008, 18(24): 3941
61. A. L. M. Reddy, M. M. Shaijumon, S. R. Gowda, and P. M. Ajayan, Coaxial MnO_2/carbon nanotube array electrodes for high-performance lithium batteries, *Nano Lett.*, 2009, 9(3): 1002
62. B. Luo, B. Wang, M. Liang, J. Ning, X. Li, and L. Zhi, Reduced graphene oxide-mediated growth of uniform tin-core/carbon-sheath coaxial nanocables with enhanced lithium ion storage properties, *Adv. Mater.*, 2012, 24(11): 1405
63. S. M. Yuan, J. X. Li, L. T. Yang, L. W. Su, L. Liu, and Z. Zhou, Preparation and lithium storage performances of mesoporous Fe_3O_4@C microcapsules, *ACS Appl. Mater. Interfaces*, 2011, 3(3): 705
64. H. Wu, G. Chan, J. W. Choi, I. Ryu, Y. Yao, M. T. McDowell, S. W. Lee, A. Jackson, Y. Yang, L. Hu, and Y. Cui, Stable cycling of double-walled silicon nanotube battery anodes through solid-electrolyte interphase control, *Nat. Nanotechnol.*, 2012, 7(5): 310
65. D. W. Kim, I. S. Hwang, S. J. Kwon, H. Y. Kang, K. S. Park, Y. J. Choi, K. J. Choi, and J. G. Park, Highly conductive coaxial SnO_2-In_2O_3 heterostructured nanowires for Li ion battery electrodes, *Nano Lett.*, 2007, 7(10): 3041
66. L. Q. Mai, X. Xu, C. H. Han, Y. Z. Luo, L. Xu, Y. A. Wu, and Y. L. Zhao, Rational synthesis of silver vanadium oxides/polyaniline triaxial nanowires with enhanced electrochemical property, *Nano Lett.*, 2011, 11(11): 4992
67. S. Li, C. H. Han, L. Q. Mai, J. H. Han, X. Xu, and Y. Q. Zhu, Rational synthesis of coaxial MoO_3/PTh nanowires with improved electrochemical cyclability, *Int. J. Electrochem. Sci.*, 2011, 6: 4504
68. L. Q. Mai, F. Dong, X. Xu, Y. Z. Luo, Q. Y. An, Y. L. Zhao, J. Pan, and J. N. Yang, Cucumber-like V_2O_5/poly(3,4-ethylenedioxythiophene) & MnO_2 nanowires with enhanced electrochemical cyclability, *Nano Lett.*, 2013, 13(2): 740
69. R. Liu and S. B. Lee, MnO_2/poly(3,4-ethylenedioxythiophene) coaxial nanowires by one-step coelectrodeposition for electrochemical energy storage, *J. Am. Chem. Soc.*, 2008, 130(10): 2942
70. X. Jiang, B. Tian, J. Xiang, F. Qian, G. Zheng, H. Wang, L. Q. Mai, and C. M. Lieber, Rational growth of branched nanowire heterostructures with synthetically encoded properties and function, *Proc. Natl. Acad. Sci. USA*, 2011, 108(30): 12212
71. B. Tian, P. Xie, T. J. Kempa, D. C. Bell, and C. M. Lieber, Single-crystalline kinked semiconductor nanowire superstructures, *Nat. Nanotechnol.*, 2009, 4(12): 824
72. S. H. Ko, D. Lee, H. W. Kang, K. H. Nam, J. Y. Yeo, S. J. Hong, C. P. Grigoropoulos, and H. J. Sung, Nanoforest of hydrothermally grown hierarchical ZnO nanowires for a high efficiency dye-sensitized solar cell, *Nano Lett.*, 2011, 11(2): 666
73. J. W. Long, B. Dunn, D. R. Rolison, and H. S. White, Three-dimensional battery architectures, *Chem. Rev.*, 2004, 104(10): 4463
74. W. Zhou, C. Cheng, J. Liu, Y. Y. Tay, J. Jiang, X. Jia, J. Zhang, H. Gong, H. H. Hng, T. Yu, and H. J. Fan, Epitaxial growth of branched –Fe_2O_3/SnO_2 nano-heterostructures with improved lithium-ion battery performance, *Adv. Funct. Mater.*, 2011, 21(13): 2439
75. J. Liu, J. Jiang, M. Bosman, and H. J. Fan, Three-dimensional tubular arrays of MnO_2-NiO nanoflakes with high areal pseudocapacitance, *J. Mater. Chem.*, 2012, 22(6): 2419
76. J. Liu, J. Jiang, C. Cheng, H. Li, J. Zhang, H. Gong, and H. J. Fan, Co_3O_4 nanowire@MnO_2 ultrathin nanosheet core/shell arrays: A new class of high-performance pseudocapacitive materials, *Adv. Mater.*, 2011, 23(18): 2076
77. L. Yang, S. Wang, J. Mao, J. Deng, Q. Gao, Y. Tang, and O. G. Schmidt, Hierarchical MoS2/polyaniline nanowires with excellent electrochemical performance for lithium-ion batteries, *Adv. Mater.*, 2013, 25(8): 1180
78. J. Zhao, Z. Lu, M. Shao, D. Yan, M. Wei, D. G. Evans, and X. Duan, Flexible hierarchical nanocomposites based on MnO_2 nanowires/CoAl hydrotalcite/carbon fibers for high-performance supercapacitors, *RSC Adv.*, 2012, 3(4): 1045
79. S. Zhou, X. Yang, Y. Lin, J. Xie, and D. Wang, A nanonet-enabled Li ion battery cathode material with high power rate, high capacity, and long cycle lifetime, *ACS Nano*, 2012, 6(1): 919
80. S. He, X. Hu, S. Chen, H. Hu, M. Hanif, and H. Hou, Needle-like polyaniline nanowires on graphite nanofibers: Hierarchical micro/nano-architecture for high performance supercapacitors, *J. Mater. Chem.*, 2012, 22(11): 5114
81. J. G. Kim, S. H. Nam, S. H. Lee, S. M. Choi, and W. B. Kim, SnO_2 nanorod-planted graphite: An effective nanostructure configuration for reversible lithium ion storage, *ACS Appl. Mater. Interfaces*, 2011, 3(3): 828

82. L. Q. Mai, F. Yang, Y. L. Zhao, X. Xu, L. Xu, and Y. Z. Luo, Hierarchical $MnMoO_4/CoMoO_4$ heterostructured nanowires with enhanced supercapacitor performance, *Nat. Commun.*, 2011, 2: 381
83. F. Schüth, Non-siliceous mesostructured and mesoporous materials, *Chem. Mater.*, 2001, 13(10): 3184
84. M. E. Davis, Ordered porous materials for emerging applications, *Nature*, 2002, 417(6891): 813
85. F. Schüth and W. Schmidt, Microporous and mesoporous materials, *Adv. Eng. Mater.*, 2002, 4(5): 269
86. C. Liang, Z. Li, and S. Dai, Mesoporous carbon materials: Synthesis and modification, *Angew. Chem. Int. Ed.*, 2008, 47(20): 3696
87. A. Corma, From microporous to mesoporous molecular sieve materials and their use in catalysis, *Chem. Rev.*, 1997, 97(6): 2373
88. J. Lee, J. Kim, and T. Hyeon, Recent progress in the synthesis of porous carbon materials, *Adv. Mater.*, 2006, 18(16): 2073
89. F. D. Wu and Y. Wang, Self-assembled echinus-like nanostructures of mesoporous CoO nanorod@CNT for lithium-ion batteries, *J. Mater. Chem.*, 2011, 21(18): 6636
90. H. Jiang, J. Ma, and C. Li, Hierarchical porous $NiCo_2O_4$ nanowires for high-rate supercapacitors, *Chem. Commun.*, 2012, 48(37): 4465
91. D. Yu, C. Chen, S. Xie, Y. Liu, K. Park, X. Zhou, Q. Zhang, J. Li, and G. Cao, Mesoporous vanadium pentoxide nanofibers with significantly enhanced Li-ionstorage properties by electrospinning, *Energy Environ. Sci.*, 2011, 4(3): 858
92. L. Q. Mai, L. Xu, C. H. Han, X. Xu, Y. Z. Luo, S. Y. Zhao, and Y. L. Zhao, Electrospun ultralong hierarchical vanadium oxide nanowires with high performance for lithium ion batteries, *Nano Lett.*, 2010, 10(11): 4750
93. Y. L. Zhao, L. Xu, L. Q. Mai, C. H. Han, Q. Y. An, X. Xu, X. Liu, and Q. J. Zhang, Hierarchical mesoporous perovskite $La_{0.5}Sr_{0.5}CoO_{2.91}$ nanowires with ultrahigh capacity for Li-air batteries, *Proc. Natl. Acad. Sci. USA*, 2012, 109(48): 19569
94. G. M. Koenig, Jr., I. Belharouak, H. X. Deng, Y. K. Sun, and K. Amine, Composition-tailored synthesis of gradient transition metal precursor particles for lithium-ion battery cathode materials, *Chem. Mater.*, 2011, 23(7): 1954
95. Y. K. Sun, S. T. Myung, B. C. Park, J. Prakash, I. Belharouak, and K. Amine, High-energy cathode material for long-life and safe lithium batteries, *Nat. Mater.*, 2009, 8(4): 320
96. Y. K. Sun, Z. Chen, H. J. Noh, D. J. Lee, H. G. Jung, Y. Ren, S. Wang, C. S. Yoon, S. T. Myung, and K. Amine, Nanostructured high-energy cathode materials for advanced lithium batteries, *Nat. Mater.*, 2012, 11(11): 942
97. R. Krishnan, T. M. Lu, and N. Koratkar, Functionally strain-graded nanoscoops for high power Li-ion battery anodes, *Nano Lett.*, 2011, 11(2): 377
98. J. Jiang, Y. Li, J. Liu, and X. Huang, Building one-dimensional oxide nanostructure arrays on conductive metal substrates for lithium-ion battery anodes, *Nanoscale*, 2011, 3(1): 45
99. C. K. Chan, H. Peng, G. Liu, K. McIlwrath, X. F. Zhang, R. A. Huggins, and Y. Cui, High-performance lithium battery anodes using silicon nanowires, *Nat. Nanotechnol.*, 2008, 3(1): 31
100. P. Meduri, E. Clark, J. H. Kim, E. Dayalan, G. U. Sumanasekera, and M. K. Sunkara, MoO_{3-x} nanowire arrays as stable and high-capacity anodes for lithium ion batteries, *Nano Lett.*, 2012, 12(4): 1784
101. S. Chen, M. Wang, J. Ye, J. Cai, Y. Ma, H. Zhou, and L. Qi, Kinetics-controlled growth of aligned mesocrystalline SnO_2 nanorod arrays for lithium-ion batteries with superior rate performance, *Nano Res.*, 2013, 6(4): 243
102. K. Wang, Q. Meng, Y. Zhang, Z. Wei, and M. Miao, High-performance two-ply yarn supercapacitors based on carbon nanotubes and polyaniline nanowire arrays, *Adv. Mater.*, 2013, 25(10): 1494
103. L. Shen, E. Uchaker, X. Zhang, and G. Cao, Hydrogenated $Li_4Ti_5O_{12}$ nanowire arrays for high rate lithium ion batteries, *Adv. Mater.*, 2012, 24(48): 6502
104. F. F. Cao, J. W. Deng, S. Xin, H. X. Ji, O. G. Schmidt, L. J. Wan, and Y. G. Guo, Cu-Si nanocable arrays as high-rate anode materials for lithium-ion batteries, *Adv. Mater.*, 2011, 23(38): 4415
105. C. H. Han, Y. Q. Pi, Q. Y. An, L. Q. Mai, J. L. Xie, X. Xu, L. Xu, Y. L. Zhao, C. J. Niu, A. M. Khan, and X. He, Substrate-assisted self-organization of radial –$AgVO_3$ nanowire clusters for high rate rechargeable lithium batteries, *Nano Lett.*, 2012, 12(9): 4668
106. L. Q. Mai, Y. H. Gu, C. H. Han, B. Hu, W. Chen, P. Zhang, L. Xu, W. L. Guo, and Y. Dai, Orientated Langmuir–Blodgett assembly of VO_2 nanowires, *Nano Lett.*, 2009, 9(2): 826